onstrated that the presence of increased OEF is a predictor of subsequent ischemic stroke;[5,6,24] however, the presence of increased OEF does not prove the actual cause of TIA because embolic TIAs can certainly occur in patients with hemodynamic cerebrovascular compromise? Given that hemodynamic CVD affects only a minority of patients with major cerebral artery occlusive lesions, the combination of clinical symptoms and hemodynamic measurement, especially OEF, is presumably the most reliable way of identifying hemodynamic CVD. However, the association between clinical symptoms and OEF has not been carefully examined. Although reduction of CBF and CBF/CBV in the frontal to parietal lobe has been reported[9,11,26] 2 recent studies in patients with ICA occlusion showed no significant differences between patients with and without hemodynamic TIA in any of the hemodynamic parameters on either MRA or in $CO_2$ reactivity measurement with TCD?[27,28]

We used the HUT test to decrease blood pressure safely for the purpose of selecting candidates for EC-IC bypass surgery. Although Tatemichi et al used infusion of trimethaphan to induce hypotension in a patient with bilateral carotid occlusive disease;[11] we prefer orthostatic stress because of the prompt recovery of blood pressure and relief from symptoms by head-down. All 3 patients who were positive in the HUT tests showed misery perfusion on PET (Table 1) and were regarded as having hemodynamic CVD, requiring referral to a neurosurgeon for EC-IC bypass. Increased OEF was observed in 2 of 9 patients without focal signs during the HUT tests and it is unknown whether these patients are at high risk of a hemodynamic incident. The presence of misery perfusion has been shown in longitudinal studies to increase the risk;[5,6] but it is unclear whether the symptoms of these patients are of hemodynamic origin or not?[5,6]

In conclusion, the HUT test was able to detect patients with cerebral hemodynamic insufficiency and the combination of the HUT test and cerebral hemodynamic measurement could be useful as an operation indication for EC-IC bypass.

## References


1. Klijn CJM, Kappelle LJ, Tulleken CAF, van Gijn J. Symptomatic carotid artery occlusion: A reappraisal of hemodynamic factors. *Stroke* 1997; **28:** 2084–2093.
2. Derdeyn CP, Grubb RL, Powers WJ. Cerebral hemodynamic inpairment: Methods of measurement and association with stroke risk. *Neurology* 1999; **53:** 251–259.
3. Hankey GJ, Warlow CP. Prognosis of symptomatic carotid artery occlusion: An overview. *Cerebrovasc Dis* 1991; **1:** 245–256.
4. Baron JC, Bousser MG, Rey A, Guillard A, Comar D, Castaigne P. Reversal of focal "misery-perfusion syndrome" by extra-intracranial arterial bypass in hemodynamic cerebral ischemia: A case study with $^{15}O$ positron emission tomography. *Stroke* 1981; **12:** 454–459.
5. Grubb RL, Derdeyn CP, Fritsch SM, Carpenter DA, Yundt KD, Videen TO, et al. Importance of hemodynamic factors in the prognosis of symptomatic carotid occlusion. *JAMA* 1998; **280:** 1055–1060.
6. Yamauchi H, Fukuyama H, Nagahama Y, Nabatame H, Ueno M, Nishizawa S, et al. Significance of increased oxygen extraction fraction in five-year prognosis of major cerebral arterial occlusive diseases. *J Nucl Med* 1999; **40:** 1992–1998.
7. Powers WJ. Cerebral hemodynamics in ischemic cerebrovascular disease. *Ann Neurol* 1991; **29:** 231–240.
8. Carey BJ, Manktelow BN, Panerai RB, Potter JF. Cerebral autoregulation responses to head-up tilt in normal subjects and patients with recurrent vasovagal syncope. *Circulation* 2001; **104:** 898–902.
9. Yanagihara T, Piepgras DG, Klass DW. Repetitive involuntary movement associated with episodic cerebral ischemia. *Ann Neurol* 1985; **18:** 244–250.
10. Baquis GD, Pessin MS, Scott RM. Limb shaking: A carotid TIA. *Stroke* 1985; **16:** 444–448.
11. Tatemichi TK, Young WL, Prohovnik I, Gitelman DR, Correll JW, Mohr JP. Perfusion insufficiency in limb-shaking transient ischemic attacks. *Stroke* 1990; **21:** 341–347.
12. Whisnant JP, Basford JR, Bernstein EF. Classification of cerebrovascular disease III. *Stroke* 1990; **21:** 637–676.
13. Shimizu Y, Kitagawa K, Nagai Y, Narita M, Hougaku H, Masuyama T, et al. Carotid atherosclerosis as a risk factor for complex aortic lesions in patients with ischemic cerebrovascular disease. *Circ J* 2003; **67:** 597–600.
14. Matsushita K, Kuriyama Y, Nagatsuka K, Nakamura M, Sawada T, Omae T. Periventricular white matter lucency and cerebral blood flow autoregulation in hypertensive patients. *Hypertension* 1994; **23:** 565–568.
15. Novak V, Novak P, Spies JM, Low PA. Autoregulation of cerebral blood flow in orthostatic hypotension. *Stroke* 1998; **29:** 104–111.
16. Dan DD, Hoag JB, Ellenbogen KA, Wood MA, Eckberg DL, Gilligan DM. Cerebral blood flow velocity declines before arterial pressure in patients with orthostatic vasovagal presyncope. *J Am Coll Cardiol* 2002; **39:** 1039–1045.
17. Suwa S, Sumiyoshi M, Mineda Y, Ohta H, Kojima S, Nakata Y. Vasovagal response induced by a low dose of isoproterenol infusion before tilting-up. *Circ J* 2004; **68:** 876–877.
18. Richardson DA, Bexton R, Shaw FE, Steen N, Bond J, Kenny RA. Complications of carotid sinus massage: A prospective series of older patients. *Age Ageing* 2000; **29:** 413–417.
19. Imaizumi M, Kitagawa K, Hashikawa K, Oku N, Teratani T, Takasawa M, et al. Detection of misery perfusion with split-dose $^{123}I$-iodoamphetamine single-photon emission computed tomography in patients with carotid occlusive diseases. *Stroke* 2002; **33:** 2217–2223.
20. The EC-IC Bypass Study Group. Failure of extracranial–intracranial arterial bypass to reduce the risk of ischemic stroke: Results of an international randomized trial. *N Engl J Med* 1985; **313:** 1191–1200.
21. Yokota C, Hasegawa Y, Minematsu K, Yamaguchi T. Effect of acetazolamide reactivity and long-term outcome in patients with major cerebral artery occlusive diseases. *Stroke* 1998; **29:** 640–644.
22. Kuroda S, Houkin K, Kamiyama H, Mitsunori K, Iwasaki Y, Abe H. Long-term prognosis of medically treated patients with internal carotid or middle cerebral artery occlusion: Can acetazolamide test predict it? *Stroke* 2001; **32:** 2110–2116.
23. Ogasawara K, Ogawa A, Terasaki K, Shimizu H, Tominaga T, Yoshimoto T. Use of cerebrovascular reactivity in patients with symptomatic major cerebral artery occlusion to predict 5-year outcome: Comparison of xenon-133 and iodine-123-IMP single-photon emission computed tomography. *J Cereb Blood Flow Metab* 2002; **22:** 1142–1148.
24. Derdeyn CP, Videen TO, Yundt KD, Fritsch SM, Carpenter DA, Grubb RL, et al. Variability of cerebral blood volume and oxygen extraction: Stages of cerebral hemodynamic impairment revisited. *Brain* 2002; **125:** 595–607.
25. Markus H, Cullinane M. Severely impaired cerebrovascular reactivity predicts stroke and TIA risk in patients with carotid artery stenosis and occlusion. *Brain* 2001; **124:** 457–467.
26. Gibbs JM, Wise RJS, Leeders KL, Jones T. Evaluation of cerebral perfusion reserve in patients with carotid-artery occlusion. *Lancet* 1984; **1:** 310–314.
27. van Everdingen KJ, Visser GH, Klijin CJM, Kappelle LJ, van der Grond J. Role of collateral flow on cerebral hemodynamics in patients with unilateral internal carotid artery occlusion. *Ann Neurol* 1998; **44:** 167–176.
28. Klijn CJM, Kappelle LJ, van der Grond J, Visser GH, Algra A, Tulleken CAF, et al. Lack of evidence for a poor haemodynamic or metabolic state of the brain in patients with haemodynamic clinical features associated with carotid artery occlusion. *Cerebrovasc Dis* 2001; **12:** 99–107.

*Circ J* 2005; **69:** 1147–1149

# Embolic Cerebral Infarction Caused by Intraluminal Thrombus in the Carotid Siphon Successfully Treated With Combination of Anticoagulant and Antiplatelet Drugs

Hiroshi Yamagami, MD*; Kazuo Kitagawa, MD; Toshiho Ohtsuki, MD**; Masayasu Matsumoto, MD†; Masatsugu Hori, MD

A 54-year-old-man experienced serial ischemic embolic strokes and retinal artery embolism in the left carotid territory. In the acute phase, intraluminal thrombus in the left carotid siphon and frequent microembolic signals (MES) in the left middle cerebral artery were detected with magnetic resonance angiography (MRA) and transcranial Doppler (TCD). The patient was initially treated with only heparin for 3 days; however, more than 30 MES per 30 min were still detected. After adding ticlopidine as an antiplatelet therapy, MES were suppressed completely. After starting combination therapy of heparin (later warfarin) and ticlopidine, repeated MRA confirmed resolution of carotid thrombus and ischemic stroke did not recur. For management of intraluminal thrombus in the carotid artery, MES with TCD was useful in evaluating the risk of distal embolism. Combination treatment with anticoagulants and ticlopidine can both resolve the thrombus and prevent distal embolism. (*Circ J* 2005; **69:** 1147–1149)

**Key Words:** Anticoagulants; Antiplatelet therapy; Cerebral embolism; Intraluminal thrombus; Trancranial Doppler

Intraluminal thrombus in the carotid artery is identified in less than 3% of patients who undergo cerebral angiography for investigation of ischemic cerebrovascular symptoms[1,2] Carotid thrombi are usually associated with atherosclerotic stenotic lesions in the carotid bifurcation. To prevent recurrent stroke in these patients, the inhibition of distal embolism must be successful in addition to the resolution of intraluminal thrombus and surgical manipulation for stenotic lesion. The risk of distal embolism can be evaluated as a microembolic signals (MES) in transcranial Doppler (TCD) sonography[3] Previous studies recommended anticoagulation for the resolution of intraluminal thombus, however, the significance of antiplatelet drugs has been rarely evaluated[4]

We report a patient with recurrent ischemic stroke and retinal artery embolism in whom intraluminal thrombus in the carotid siphon and frequent MES in the middle cerebral artery (MCA) were successfully resolved with combination therapy of anticoagulant and antiplatelet drugs.

*(Received April 18, 2005; revised manuscript received May 23, 2005; accepted June 15, 2005)*

*Division of Strokology, Department of Cardiovascular Medicine (A8), Osaka University Graduate School of Medicine, Suita, *Department of Neurology, Stroke Center, Kobe City General Hospital, Kobe, **Department of Cerebrovascular Disease, National Cardiovascular Center, Suita and †Department of Clinical Neuroscience and Therapeutics, Hiroshima Graduate School of Biomedical Sciences, Hiroshima, Japan*

Mailing address: Kazuo Kitagawa, MD, Division of Strokology, Department of Cardiovascular Medicine (A8), Osaka University Graduate School of Medicine, 2-2 Yamada-oka, Suita 565-0871, Japan. E-mail: kitagawa@medone.med.osaka-u.ac.jp

## Case Report

A 54-year-old man experienced right-hand numbness and difficulties with reading and writing in May 2000. A brain computed tomography revealed a low-density area with partial high density in the left parieto-temporal lobe. On admission to hospital in June, the patient's physical examination was normal and neurological examination revealed right-lower quadrantanopsia, slight right hemiparesis and sensory aphasia.

Three weeks later, the patient suddenly developed a loss of vision in the left eye and became confused. Funduscopic examinations revealed branch occlusion of the left retinal artery. Laboratory tests showed the following abnormalities: thrombin-antithrombin III complex, 4.48 μg/L (normal range, 0-3.0); D-dimer, 1.18 μg/ml (0-0.50); β-thromboglobulin, 473 ng/ml (<50); and platelet factor-4, 115 ng/ml (<20). Prothrombin time, activated partial thrombin time (APTT), protein S and C, anticardiolipin antibody and lupus anticoagulant were all within normal limits.

Diffusion-weighted magnetic resonance imaging (MRI) showed small hyperintensity regions scattered within the left MCA territory (Fig 1A). Magnetic resonance angiography (MRA) revealed intraluminal thrombus in the cavernous portion of the left internal carotid artery (Fig 1C). TCD monitoring detected 53 MES over 30 min in the left MCA. To determine the embolic source, the following examinations were performed and showed normal findings: electrocardiogram (ECG), Holter ECG and transthoracic echocardiography. Carotid ultrasonography showed no atheromatous lesion in the carotid bifurcation. In transesophageal echocardiography (TEE), thrombus in the left atrium or patent foramen ovale was not detected, but an

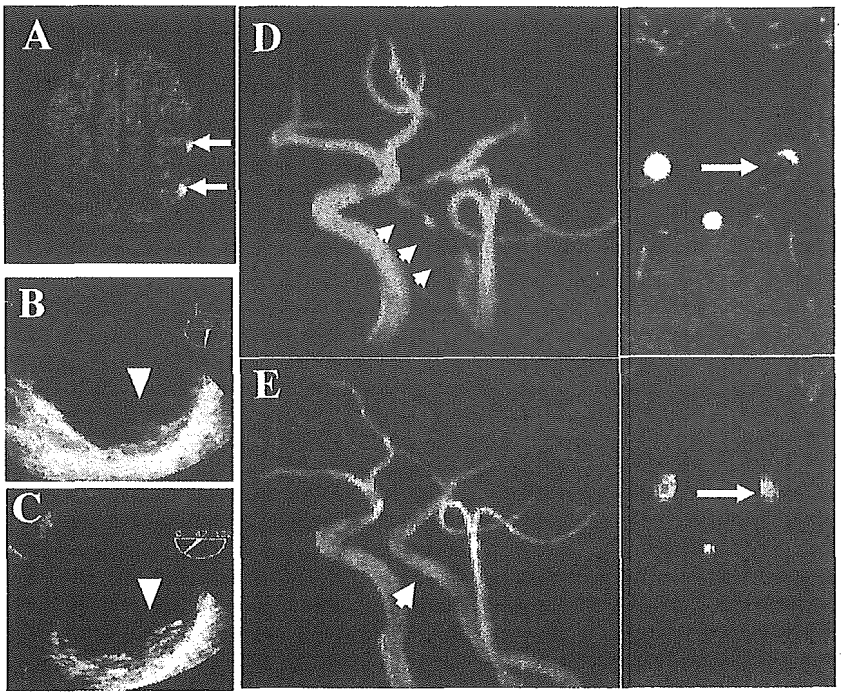


Fig 1. Diffusion weighted images (DWI) of the magnetic resonance imaging (A), transverse images of aortic arch obtained using transesophageal echocadgiography (TEE) (B,C), maximum-intensity projection images (Left) and source images (Right) of the magnetic resonance angiography (D, E). (A) DWI images showing scattered regions of hyperintensity in the left middle cerebral artery territory. (B) Atheromatous plaque with a mobile component (arrowhead) in the aortic arch on TEE. (C) A week after anticoagulation therapy, the mobile component has almost disappeared (arrowhead). (D) An intraluminal filling defect in the left carotid siphon can be seen (arrowheads). Round and concentric defects are typical of an intraluminal thrombus (arrow). (E) Resolution of the intraluminal thrombus (arrow and arrowhead) after combination therapy with anticoagulant and antiplatelet drugs.

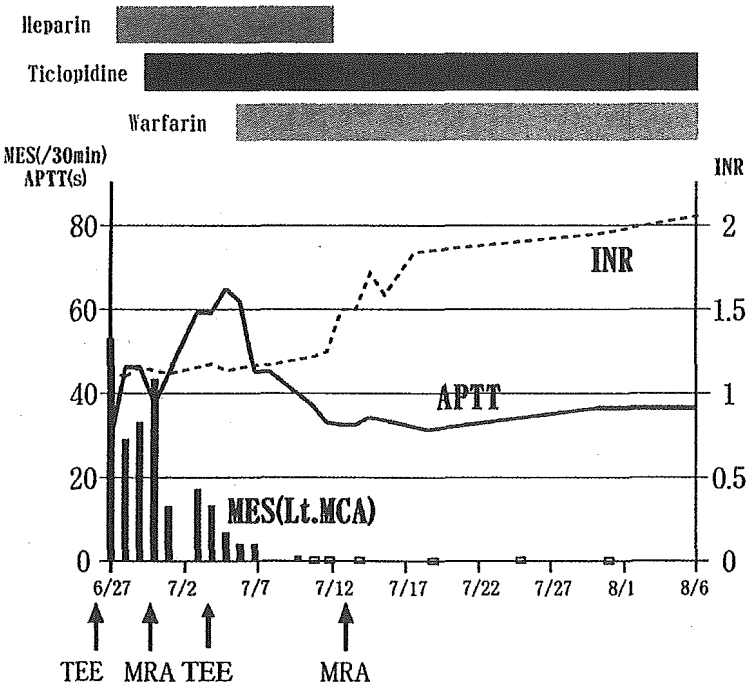


Fig 2. Time course of microembolic signals (MES) in transcranial Doppler with anticoagulation (heparin or warfarin) and antiplatelet therapy (ticlopidine). The number of MES in the left middle cerebral artery is shown as embolus per 30 min. The white box on the baseline indicates no embolic signal. Activated partial thrombin time (APTT) and international normalized ratio (INR) are shown as solid and dotted lines respectively. MCA, middle cerebral artery; TEE, transesophageal echocadgiography; MRA, magnetic resonance angiography.

atherosclerotic plaque protruding in the aortic arch with a mobile component was found (Fig 1B). We diagnosed cerebral and retinal embolism due to intraluminal thrombus in the carotid siphon. The potential cause of intraluminal thrombus was aortic complex lesions.

The patient was soon treated with heparin intravenously (12,000 U/day); however, TCD monitoring for MES showed more than 30 emboli in spite of effective anticoagulation treatment as judged with APTT (Fig 2). To prevent distal embolism, we started treatment with ticlopidine as an antiplatelet strategy in combination with anticoagulant. Thereafter, serial TCD monitoring showed a marked decrease of the MES in the left MCA. A week after starting anticoagulation therapy, repeated TEE showed resolution of mobile components in an atherosclerotic plaque (Fig 1C). We continued combination therapy of anticoaguilant and antiplatelet drugs after replacement of heparin by warfarin. Two weeks after starting combination therapy, repeated MRA revealed the resolution of intraluminal thrombus in the left carotid siphon (Fig 1D). The patient recovered consciousness within 1 week of starting treatment and the aphasia diminished by the end of July. He was discharged

for normal daily activities the next month.

## Discussion

In the present case, we successfully treated high-risk patient with intraluminal thrombus in the carotid siphon using a combination of anticoagulant and antiplatelet therapy. In terms of diagnosis, we first had to rule out the possibility of carotid dissection. Carotid dissection was highly unlikely in the present case based on the following findings: although the typical indicator of dissection on MRI is a narrowed lumen surrounded by crescent and eccentric hyperintense signal, in the present case the filling defect was round and concentric (Fig 1D, arrow).[5] Dissection usually terminates before the petrous portion and in the present case the filling defect was seen at the carotid siphon. Furthermore, the present case had multiple ischemic events, although the recurrence of dissections in the same artery is rare.

Intraluminal thrombus is usually associated with an advanced atherosclerotic lesion in the carotid bifurcation.[1,2,6] Cardiac embolic sources may also cause an intraluminal carotid thrombus. In the present case, we failed to detect an atherosclerotic lesion in the carotid bifurcation or another embolic source including: the left atrial thrombus, patent foramen ovale or paroxysmal atrial fibrillation. Other possible causes of hypercoagulability were not found, aside from an activated platelet function.[7] Therefore, an atheromatous plaque with a mobile component in the aortic arch could be the only embolic source in this patient. Several papers have reported TEE recognition of aortic atheroma as the potential source of embolic stroke.[8,9]

The novel finding in the present case was the possibility that ticlopidine suppressed MES from an intraluminal thrombus. We used ticlopidine in expectation of a stronger antiplatelet effect than aspirin because a randomized trial in high-risk patients demonstrated that ticlopidine was somewhat more effective than aspirin in preventing stroke.[10] The detection of MES is potentially useful for identifying acute stroke patients at high risk of recurrent stroke or evaluating the effectiveness of anticoagulant or antiplatelet therapies in these patients.[11,12] In the present case, frequent MES were still detected after anticoagulant therapy but only suppressed after the administration of ticlopidine. There is no doubt that anticoagulants are effective in the resolution of carotid thrombus.[2,4] However, the role of antiplatelet therapy has not been clearly demonstrated. Our findings suggest the importance of antiplatelet therapy for the suppression of distal embolism due to intraluminal thrombus. The patient received a combination of ticlopidine and warfarin for the prevention of recurrent stroke at discharge. The ongoing Aortic arch Related Cerebral Hazard study may determine whether or not antiplatelet drugs are more effective than anticoagulation alone.[13] The present findings demonstrate the usefulness of TCD monitoring in the assessment of distal embolism in intraluminal thrombus and of the recommended combination of anticoagulant and antiplatelet drugs for the resolution of thrombus and prevention of recurrent stroke.

*Acknowledgments*

*The present study was supported in part by the Smoking Research Foundation of Japan. The authors wish to thank Miss Aki Kanzawa and Miss Sizuka Higa for their assistance with the manuscript.*

## References

1. Biller J, Adams HP Jr, Boarini D, Godersky JC, Smoker WR, Kongable G. Intraluminal clot of the carotid artery: A clinical-angiographic correlation of nine patients and literature review. *Surg Neurol* 1986; **25:** 467–477.
2. Buchan A, Gates P, Pelz D, Barnett HJ. Intraluminal thrombus in the cerebral circulation: Implications for surgical management. *Stroke* 1988; **19:** 681–687.
3. Molloy J, Matkus HS. Asymptyomatic embolization predicts stroke and TIA risk in patients with carotid artery stenosis. *Stroke* 1999; **30:** 1440–1443.
4. Pelz DM, Buchan A, Fox AJ, Barnett HJ, Vinuela F. Intraluminal thrombus of the internal carotid arteries: Angiographic demonstration of resolution with anticoagulant therapy alone. *Radiology* 1986; **160:** 369–373.
5. Schevink WI. Spontaneous dissection of the carotid and vertebral arteries. *N Engl J Med* 2001; **344:** 898–906.
6. Gonzalez A, Mayol A, Gil-Peralta A, Gonzalez-Marcos JR, Boza F, Ruano J. Angioplasty of symptomatic high-grade internal carotid artery stenosis with intraluminal thrombus: Therapeutic approach. *Neuroradiology* 2004; **46:** 313–317.
7. Pessin MS, Abbott BP, Prager RJ, Batson RA, Scott RM. Clinical and angiographic features of carotid circulation thrombus. *Neurology* 1986; **36:** 518–523.
8. Tunick PA, Kronzon I. Protruding atherosclerotic plaque in aortic arch of patients with systemic embolization: A new finding seen by transesophageal echocardiography. *Am Heart J* 1990; **124:** 658–660.
9. Shimizu Y, Kitagawa K, Nagai Y, Narita M, Hougaku H, Masuyama T, et al. Carotid atherosclerosis as a risk factor for complex aortic lesions in patients with ischemic cerebrovascular disease. *Circ J* 2003; **67:** 597–600.
10. Hass WK, Easton JD, Adams HP Jr, Pryse-Phillips W, Molony BA, Anderson S, et al. A randomized trial comparing ticlopidine hydrochloride with aspirin for the prevention of stroke in high-risk patients. *N Engl J Med* 1989; **321:** 501–507.
11. Valton L, Larrue V, le Traon AP, Massabuau P, Geraud G. Microembolic signals and risk of early recurrence in patients with stroke or transient ischemic attack. *Stroke* 1998; **29:** 2125–2128.
12. Kaposzta Z, Young E, Bath PM, Markus HS. Clinical application of asymptomatic embolic signal detection in acute stroke: A prospective study. *Stroke* 1999; **30:** 1814–1818.
13. Donnan GA, Davis SM, Jones EF, Amarenco P. Aortic source of brain embolism. *Curr Treat Options Cardiovasc Med* 2003; **5:** 211–219.

THE JOURNAL OF BIOLOGICAL CHEMISTRY
Vol. 280, No. 32, Issue of August 12, pp. 29096–29106, 2005
Printed in U.S.A.


# Mutant Protein Kinase Cγ Found in Spinocerebellar Ataxia Type 14 Is Susceptible to Aggregation and Causes Cell Death*[S]

Received for publication, February 15, 2005, and in revised form, June 15, 2005
Published, JBC Papers in Press, June 17, 2005, DOI 10.1074/jbc.M501716200

**Takahiro Seki‡, Naoko Adachi§, Yoshitaka Ono¶, Hideki Mochizuki‡‖, Keiko Hiramoto‡**, Taku Amano‡, Hiroaki Matsubayashi‡, Masayasu Matsumoto‡‡, Hideshi Kawakami‡‡, Naoaki Saito§, and Norio Sakai‡§§**

*From the ‡Department of Molecular and Pharmacological Neuroscience, the ‖Department of Ophthalmology and Visual Sciences, the **Department of Neurosurgery, and the ‡‡Department of Clinical Neuroscience and Therapeutics, Graduate School of Biomedical Sciences, Hiroshima University, Hiroshima 734-8551, Japan and the §Laboratory of Molecular Pharmacology and ¶Biosignal Research Center, Kobe University, Kobe 657-8501, Japan*

**Spinocerebellar ataxia type 14 (SCA14) is an autosomal dominant neurodegenerative disease characterized by various symptoms including cerebellar ataxia. Recently, several missense mutations in the protein kinase Cγ (*γPKC*) gene have been found in different SCA14 families. To elucidate how the mutant γPKC causes SCA14, we examined the molecular properties of seven mutant (H101Y, G118D, S119P, S119F, Q127R, G128D, and F643L) γPKCs fused with green fluorescent protein (γPKC-GFP). Wild-type γPKC-GFP was expressed ubiquitously in the cytoplasm of CHO cells, whereas mutant γPKC-GFP tended to aggregate in the cytoplasm. The insolubility of mutant γPKC-GFP to Triton X-100 was increased and correlated with the extent of aggregation. γPKC-GFP in the Triton-insoluble fraction was rarely phosphorylated at Thr$^{514}$, whereas γPKC-GFP in the Triton-soluble fraction was phosphorylated. Furthermore, the stimulation of the P2Y receptor triggered the rapid aggregation of mutant γPKC-GFP within 10 min after transient translocation to the plasma membrane. Overexpression of the mutant γPKC-GFP caused cell death that was more prominent than wild type. The cytotoxicity was exacerbated in parallel with the expression level of the mutant. These results indicate that SCA14 mutations make γPKC form cytoplasmic aggregates, suggesting the involvement of this property in the etiology of SCA14.**

The autosomal dominant spinocerebellar ataxias (SCAs)[1] are a heterogeneous group of neurological disorders clinically characterized by progressive ataxia of gait and limbs, cerebellar dysarthria, abnormal eye movements, and so on. SCAs are classified at least into 25 types (SCA1–8, 10–19, 21–23, 25, 26 DRPLA, FGF14) by genetic patterns, clinical features, and pathological findings (1, 2). The genes involved and the responsible mutations have been identified in several types of SCAs. Among these, CAG trinucleotide repeat expansions are commonly found in seven types (SCA1, 2, 3, 6, 7, 17 and DRPLA) (1, 2). Diseases caused by such expansions, including Huntington disease and spinal and bulbar muscular atrophy (SBMA), are called polyglutamine diseases (3, 4). The aggregation of mutant proteins having an abnormally elongated polyglutamine tract is considered to be the molecular basis of neuronal degeneration in polyglutamine diseases (5).

Recently, six different missense mutations in protein kinase Cγ (*γPKC*) gene (*PRKCG*) have been found in SCA14 families (6–9). Five mutations are located in exon 4, encoding the C1B region in the regulatory domain of γPKC, and one mutation is in exon 18, encoding the C terminus of the catalytic domain of γPKC (Fig. 1). Furthermore, we found a novel mutation in a Japanese SCA14 family (Fig. 1, *bold lined box*).[2] Because mutations associated with SCA14 affect highly conserved amino acids among the PKC family members, it is possible that these mutations disturb the fundamental function or conformation of γPKC. However, how these mutations cause cerebellar degeneration remains controversial.

PKC is a family of serine/threonine kinases which plays important roles in signal transduction and the regulation of various cellular functions. Among PKC subtypes, γPKC is specifically present in the central nervous system and is especially abundant in cerebellar Purkinje cells and hippocampal pyramidal cells (10). Therefore, γPKC is thought to be involved in various neuronal functions including synaptic plasticity and memory via modulating long term potentiation and long term depression (11). γPKC knock-out mice showed mildly impaired motor coordination and incomplete developmental elimination of synapses between Purkinje cell and climbing fibers (12, 13). Furthermore, in model mice of SCA1 overexpressing mutant ataxin-1 with elongated polyglutamine, γPKC was down-regulated and abnormally localized to the cytoplasmic vacuoles in Purkinje cells (14). These findings suggest that γPKC may be involved in SCA.

Previous live imaging studies using green fluorescent protein (GFP)-tagged PKC (PKC-GFP) demonstrated that PKCs are translocated to several cellular organelles in an isoform- and

* This work was supported by a grant-in-aid for Scientific Research from the Ministry of Education, Sports and Culture and by a grant from Takeda Science Foundation and the Japanese Smoking Research Association. The costs of publication of this article were defrayed in part by the payment of page charges. This article must therefore be hereby marked "*advertisement*" in accordance with 18 U.S.C. Section 1734 solely to indicate this fact.

[S] The on-line version of this article (available at http://www.jbc.org) contains a Supplemental Video.

§§ To whom correspondence should be addressed: Dept. of Molecular and Pharmacological Neuroscience, Graduate School of Biomedical Sciences, Hiroshima University, Minami-ku, 1-2-3 Kasumi, Hiroshima 734-8551, Japan. Tel.: 81-82-257-5142; Fax: 81-82-257-5144; E-mail: nsakai@hiroshima-u.ac.jp.

[1] The abbreviations used are: SCAs, spinocerebellar ataxias; PKC, protein kinase C; CHO, Chinese hamster ovary; GFP, green fluorescent protein; RIPA, radioimmunoprecipitation assay; PVDF, polyvinylidine difluoride; NGS, normal goat serum; 7-AAD, 7-amino-actinomycin D; UPS, ubiquitin-proteasome system; PDK1, 3-phosphoinositide-dependent protein kinase-1; WGA, wheat germ agglutinin; FI/A, fluorescence intensity per area; FRAP, fluorescent recovery after photobleaching; WT, wild type; PBS, phosphate-buffered saline.

[2] K. Hiramoto, H. Kawakami, K. Inoue, T. Seki, H. Maruyama, H. Morino, M. Matsumoto, K. Kurisu, and N. Sakai, submitted data.

stimulation-specific manner when PKCs are activated by different stimulations. Thereafter, PKCs recognize and phosphorylate their substrates at the targeted subcellular regions and cause the subsequent cellular responses (PKC targeting). This PKC targeting is considered to be the molecular basis underlining the multiplicity of PKC-mediated functions. Using transgenic mice overexpressing γPKC-GFP, we have recently reported that the translocation of γPKC-GFP, which was induced by the electrical stimulation of parallel fibers, propagated along the dendritic shaft of the cerebellar Purkinje cells (15), indicating that PKC targeting is prerequisite for various PKC-involved neuronal functions in Purkinje cells.

γPKC is a member of the classical PKCs (cPKCs), which are activated by diacylglycerol (DG) and $Ca^{2+}$ in the presence of phosphatidylserine (16). γPKC has C1 and C2 domains, which bind DG and $Ca^{2+}$, respectively (17), in its regulatory domain (Fig. 1). The C1 domain of γPKC is subdivided into two cysteine-rich repeats (C1A and C1B), both of which bind with DG and phorbol ester with high affinity (18, 19). The C1 and C2 domains have crucial roles in PKC targeting through binding to these PKC activators (20). As described above, 6 of 7 missense mutations found in SCA14 families are located in the C1B domain of γPKC (Fig. 1). Therefore, it is possible that these missense mutations influence the targeting of γPKC. In the present study, to elucidate how mutant γPKCs induced the neuronal degeneration and the pathology of SCA14, we focused on PKC targeting. We expressed mutant γPKC-GFP in culture cells and compared its localization and receptor-mediated translocation with those of wild type.

## EXPERIMENTAL PROCEDURES

*Materials*—ATP was purchased from Research Biochemical International (Natick, MA). Anti-GFP rabbit polyclonal antibody, Alexa546-conjugated anti-rabbit IgG goat antibody and Alexa633-conjugated wheat germ agglutinin (WGA) were from Molecular Probes (Leiden, Netherlands). Anti-phospho-γPKC ($Thr^{514}$), anti-phospho-γPKC($Thr^{655}$) and anti-phospho-γPKC($Thr^{674}$) polyclonal antibodies were from BIOSOURCE International (Camarillo, CA). Horseradish peroxidase-conjugated goat anti-rabbit IgG antibody was from Jackson ImmunoResearch Laboratories (West Grove, PA). Anti-γPKC polyclonal antibody was from Santa Cruz Biotechnology (Santa Cruz, CA).

*Plasmid Construction*—Human γPKC cDNA was cloned from a human cDNA library by PCR and subcloned into pBluescript II KS(+) vector (Stratagene, La Jolla, CA). Mutant human γPKC cDNAs were constructed by using QuickChange multisite-directed mutagenesis kit (Stratagene). To construct the plasmids encoding wild-type or mutant γPKC-GFP, γPKC and GFP cDNAs were together subcloned into the expression vector, pcDNA3 (Invitrogen). The GFP cDNA followed the γPKC cDNA so that GFP protein was fused with the C terminus of γPKC. All wild-type and mutant γPKC cDNAs were verified by sequencing.

*Cell Culture*—The CHO-K1 cell strain was a gift from Dr. Nishijima (National Institute of Health, Tokyo, Japan). CHO cells were cultured in Ham's F12 medium (Sigma), supplemented with 10% fetal bovine serum, 100 units/ml of penicillin, and 100 μg/ml of streptomycin in a humidified atmosphere containing 5% $CO_2$ at 37 °C.

*Immunoblotting*—Plasmids (5 μg) were transfected into CHO cells ($2 \times 10^5$ cells) by lipofection using the Fugene™6 transfection reagent (Roche Applied Science) according to the manufacturer's directions. Transfected CHO cells were spread onto 6-cm diameter dishes and cultured for 2 days. Cells were harvested by 500 × *g* centrifugation, followed by washing with 1 ml of homogenate buffer (250 mM sucrose, 10 mM EGTA, 2 mM EDTA, and 50 mM Tris-HCl, pH 7.4). For preparing total cell fractions, cells were resuspended in 100 μl of RIPA buffer (1% Nonidet P40, 0.1% sodium deoxycholate, 0.1% SDS, 150 mM NaCl, 1 mM EDTA, 20 μg/ml of leupeptin, 1 mM phenylmethylsulfonyl fluoride, 1 mM sodium orthovanadate, 1 mM NaF, and 100 nM calyculin A, and 10 mM Tris-HCl, pH 7.4) and sonicated (UR-20P, TOMY SEIKO, Tokyo, Japan) (output, 4; duty, 50%) for 15 times at 4 °C. For immunoblotting, the same amounts (10–20 μg) of samples were subjected to 7.5% SDS-PAGE, and the separated proteins were electrophoretically transferred onto polyvinylidine difluoride (PVDF) filters (Millipore, Bedford, MA). Nonspecific binding sites on PVDF filters were blocked by incubation with 5% skim milk in PBS-T (0.01 M phosphate-buffered saline containing 0.03% Triton X-100) for >1 h at room temperature. After washing with PBS-T, the PVDF filters were incubated with anti-GFP polyclonal antibody (diluted 1:2000) or anti-phospho-PKCγ ($Thr^{514}$) polyclonal antibody (diluted 1:1000) for >1 h at room temperature. After further washing, the filters were incubated with horseradish peroxidase-conjugated anti-rabbit IgG antibody (diluted 1:10,000) for >30 min at room temperature. After three more washes, the immunoreactive bands were visualized with a chemiluminescence detection kit (ECL™ Western blotting detection reagents, Amersham Biosciences) The band densities were quantified with Fluor-S MultiImager (Bio-Rad).

For preparing Triton-soluble (S) and -insoluble (I) fractions, cells were suspended in lysis buffer (homogenate buffer containing 1% Triton X-100, 20 μg/ml of leupeptin, 1 mM phenylmethylsulfonyl fluoride, 1 mM sodium orthovanadate, 1 mM NaF, and 100 nM calyculin A) and sonicated. Samples were centrifuged at 15,000 × *g* for 15 min at 4 °C, and the supernatants were collected as the S fraction. The pellets were resuspended with 50 μl of RIPA buffer, sonicated, and used as the I fraction. One-twentieth volume of each fraction was subjected to 7.5% SDS-PAGE and immunoblotted by the same method as described above.

*Observation of γPKC-GFP Localization*—CHO cells ($1 \times 10^5$ cells) were spread onto poly-D-lysine-coated glass bottom culture dishes (MatTek Corp., Ashland, MA) and were transfected with 2.5 μg of plasmid by lipofection. Transfected cells were cultured for 2 days until the observation. After the culture medium was replaced with 1 ml of HEPES buffer (135 mM NaCl, 5.4 mM KCl, 1 mM $MgCl_2$, 1.8 mM $CaCl_2$, 5 mM HEPES, and 10 mM glucose, pH 7.3), the fluorescence of GFP was monitored with a confocal laser scanning fluorescent microscope (LSM510META, Carl Zeiss, Esslingen, Germany) at 488-nm argon laser excitation using a 505–530-nm band pass barrier filter.

To analyze the expression level of wild-type or mutant γPKC-GFP in individual cells, fluorescence images of randomly selected CHO cells expressing γPKC-GFPs were obtained. For this purpose, parameters of confocal laser scanning fluorescent microscope (*e.g.* pinhole, laser intensity, and sensitivity of fluorescence) were adjusted to the same level. The fluorescence intensity and the area of the whole cell were measured using LSM510META software. The fluorescence intensity per area (FI/A) was used as an index for estimating the expression level of γPKC-GFPs in each cell.

*Fluorescent Recovery after Photobleaching (FRAP) Analysis*—Circular regions in the cytoplasm of CHO cells expressing mutant γPKC-GFP were photobleached by scanning for 15 s with an argon laser of the highest power. Before and after photobleaching, the bleached cells were monitored for 30 min.

*Observation of γPKC-GFP Translocation*—Wild-type or mutant γPKC-GFP-transfected CHO cells were cultured in glass bottom dishes for 2 days until observation. After the culture medium was replaced with 0.9 ml of HEPES buffer, the GFP fluorescence was monitored with a confocal laser scanning fluorescent microscope. Translocations of GFP-fused proteins were triggered by a direct application of 0.1 ml of ATP solution at 10× higher concentration into HEPES buffer to obtain the appropriate final concentration. Images were recorded every 5 s for 5–10 min before and after the stimulation. All experiments were performed at room temperature.

*Immunostaining and Staining with Golgi Complex Marker*—Two days after transfection, CHO cells were fixed with 4% paraformaldehyde and 0.2% picric acid in 0.1 M phosphate buffer, pH 7.4, for more than 30 min. After washing twice with PBS-T, the cells were treated with PBS containing 0.3% Triton X-100 and 5% normal goat serum (NGS) for 5 min at room temperature. For immunostaining, the cells were then incubated with the anti-γPKC polyclonal antibody (1:1000) and 5% NGS in PBS-T for 1 h at room temperature. After three times washing with PBS-T, the cells were incubated with Alexa546-conjugated goat anti-rabbit IgG antibody (1:500) and 5% NGS in PBS-T for 1 h at room temperature, followed by three washes with PBS-T. For staining with Golgi complex marker, the cells were incubated with 1 μg/ml Alexa633-conjugated WGA and 5% NGS in PBS-T for 40 min at room temperature, followed by three washes with PBS-T. The fluorescence of Alexa546 and Alexa633 was observed with a confocal scanning fluorescent microscope at 543-nm and 633-nm HeNe laser excitation using a 560-nm and 650 nm-long pass barrier filter, respectively.

*Evaluating and Counting Cells with Aggregation*—CHO cells transfected with γPKC-GFP were cultured for 2 days and fixed as described above. After two washes with PBS, cells were observed using fluorescent microscopy. We classified cells expressing γPKC-GFP into three types: cells without aggregation, with massive aggregations, and with dot-like aggregations (Fig. 2, *A–C*). We evaluated the cell type and counted the number of each cell type in 50–60 GFP-positive cells

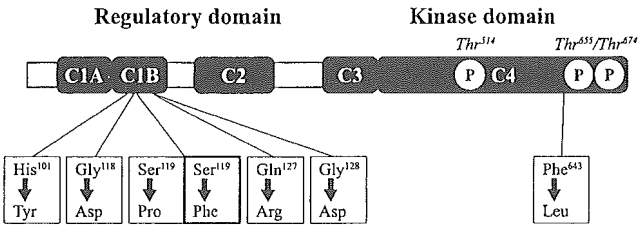


FIG. 1. **Schematic illustrations of γPKC protein and the mutated amino acid found in SCA14 families.** Seven mutations and substituted amino acids are listed in the box *below* the diagram. The *bold lined box* represents a mutation found by our group. Three phosphorylation sites are shown in *italic* above the diagram. The $Thr^{514}$ in the activation loop is phosphorylated by PDK1. The other two sites, $Thr^{655}$ and $Thr^{674}$, located near the C terminus, are autophosphorylated after PDK1 initially phosphorylates $Thr^{514}$.

*Analyzing Cell Death Using Flow Cytometry*—Flow cytometric analyses were conducted using FACSCalibur (BD Biosciences). We used 7-amino-actinomycin D (BD Biosciences) as a marker for dead cells. Transfected CHO cells were cultured on 6-cm diameter dishes for 3 days. Cells were isolated with 0.125% trypsin and 0.5 mM EDTA, washed three times, and suspended in 10 mM HEPES buffer (pH 7.4) containing 140 mM NaCl and 2.5 mM $CaCl_2$. We added 5 μl of 50 μg/ml 7-AAD into $1 \times 10^5$ cells in 100 μl of HEPES buffer and incubated cells for 10 min at room temperature. Stained cells were immediately analyzed by flow cytometry at a 488-nm argon laser excitation using a 515–545-nm band pass barrier filter for GFP and 650-nm long pass filter for 7-AAD. For each sample, the fluorescence of $2 \times 10^4$ cells was recorded and analyzed by the Cell Quest™ software (BD Biosciences).

## RESULTS

*Mutant γPKC-GFPs Tended to Aggregate in CHO Cells*—Six different missense mutations (5 around the C1 domain and 1 in the catalytic domain) have been reported in the *γPKC* gene in different SCA14 families (Fig. 1). Recently, we found a novel mutation around the C1 domain ($Ser^{119}$ replaced with Phe) of γPKC in a Japanese SCA family (Fig, 1, *bold lined box*).[2] To clarify how these mutations affect the molecular properties of γPKC and trigger neurodegeneration, we introduced these missense mutations into γPKC-GFP and investigated molecular properties of 7 mutant γPKC-GFPs (H101Y, G118D, S119P, S119F, Q127R, G128D, and F643L) expressed in CHO cells. Most of the CHO cells expressing wild-type γPKC-GFP had a ubiquitous GFP fluorescence in the cytoplasm, but not in the nucleus (Fig. 2*A*). On the other hand, cells expressing mutant γPKC-GFP frequently had aggregated GFP fluorescence in the cytoplasm (Fig. 2, *B* and *C*). Precise observation revealed that there were two patterns of mutant γPKC-GFP aggregation, massive aggregation and dot-like aggregation as described in Fig. 2, *B* and *C*, respectively. Massive aggregation was seen in the vicinity of the nucleus (Fig. 2*B*), whereas dot-like ones were seen in cytoplasm (Fig. 2*C*). Therefore, we classified aggregation patterns into these two types. We evaluated the extent of γPKC-GFP aggregations in 50–60 GFP-positive CHO cells expressing wild-type or mutant γPKC-GFP. Results are shown in Fig. 2*D*. Although wild-type γPKC-GFP aggregations were observed in 20.9 ± 2.7% of expressed cells, all seven mutants were preferably aggregated, and the percentage of cells having aggregation was over 30%. In six mutants (G118D, S119P, Q119F, Q127R, G128D, and F643L), the percentages were significantly greater than that in wild-type γPKC-GFP. In cells expressing H101Y, S119F, and F643L mutant γPKC-GFPs, massive aggregations were more often observed than in cells expressing wild type, whereas G118D, S119P, Q127R, G128D, and F643L mutants more frequently formed dot-like aggregations than wild type (Table I). Similar massive and dot-like aggregations were observed when γPKC-GFPs were expressed in other cell lines such as COS-7 and SH-SY5Y cells (data not shown).

To exclude the possibility that the aggregate formation of

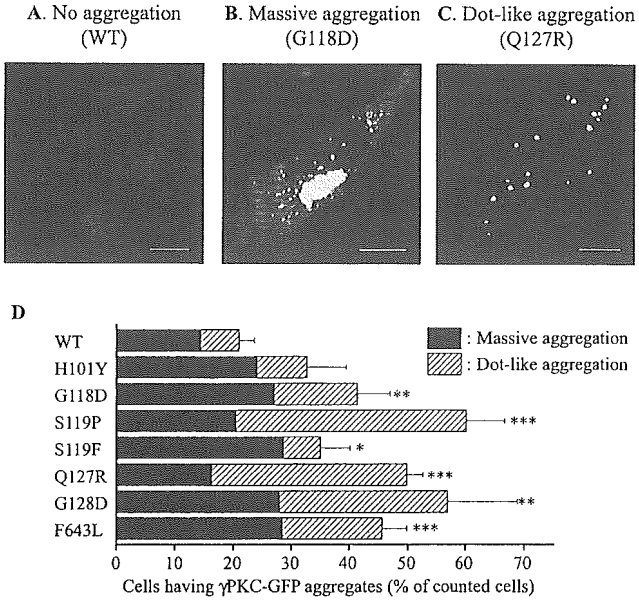


FIG. 2. **Mutant γPKC-GFPs aggregates in the cytoplasm of CHO cells in two different manners.** *A–C*, representative images of WT or mutant γPKC-GFP expression in CHO cells. *A*, WT γPKC-GFP is uniformly expressed in the cytoplasm. *B*, massive aggregation of mutant γPKC-GFP (G118D) is seen near the nucleus. *C*, dot-like aggregations of mutant γPKC-GFP (Q127R) is seen in the cytoplasm. Cells were observed using confocal laser microscope 2 days after transfection. *Bar*, 10 μm. *D*, extent of aggregation of wild-type and mutant γPKC-GFP. We evaluated 50–60 GFP-positive cells expressing wild-type or mutant γPKC-GFP. Each *bar* indicates the percentage of cells showing aggregation of wild-type or mutant γPKC-GFP. *Black* and *hatched parts* of each bar represent the percentage of cells showing massive and dot-like aggregations, respectively. *, $p < 0.05$; **, $p < 0.01$ *versus* WT (unpaired Student's *t* test, $n = 6$ in WT and S119P, $n = 5$ in S119F, $n = 4$ in other mutants).

γPKC-GFPs depends on their excessive expression, but not on the properties of mutated proteins, we investigated the relationship between the expression level and the aggregate formation of γPKC-GFP. In CHO cells expressing wild type and S119P and G128D γPKC-GFPs, fluorescent images of randomly selected 30–40 cells were obtained using the same parameters of confocal laser scanning microscope. The fluorescence intensity per area (FI/A), which represents the mean of the fluorescence intensity throughout the cell, was used as an index exhibiting the expression level of γPKC-GFPs in each cell. In Fig. 3*A*, histograms show the distribution of cells with or without aggregation classified by γPKC-GFP expression level. In wild-type γPKC-GFP, all cells with FI/A <100 did not have any aggregation (0/23 cells). Aggregations were observed only in cells with FI/A >100 (7/12 cells). In contrast, in S119P and G128D mutant γPKC-GFPs, aggregations were frequently observed in cells whose FI/A were 20–100 (22/25 cells in S119P and 19/26 cells in G128D). Fig. 3*B* shows the representative images of cells expressing wild-type and mutant (S119P and G128D) γPKC-GFPs with FI/A 40–60, indicating that the expression levels of γPKC-GFPs were similar among these three cell types. Although wild-type γPKC-GFP was uniformly expressed in the cytoplasm, mutant γPKC-GFPs formed dot-like aggregation in the cytoplasm. These results indicate that the susceptibility to aggregate formation of mutant γPKC-GFPs is determined by their properties, but not by their expression level.

Next, we examined whether massive and dot-like aggregation of γPKC-GFP were colocalized with cellular organelles. The massive aggregation of wild-type γPKC-GFP was strongly colocalized with the wheat germ agglutinin (WGA), a Golgi

TABLE I
*Properties of WT and mutant γPKC-GFPs found in the present study*
Results are represented as mean ± S.E. except aggregation after translocation, which is indicated as observed cells/examined cells.

| | WT | H101Y | G118D | S119P | S119F | Q127R | G128D | F643L |
|---|---|---|---|---|---|---|---|---|
| Cells having | | | | | | | | |
| Aggregates | 20.9 ± 2.7 | 32.7 ± 6.8 | 41.4 ± 5.6[a] | 60.2 ± 6.4[b] | 35.0 ± 5.2[c] | 49.8 ± 2.7[b] | 56.9 ± 11.9[a] | 45.6 ± 4.3[b] |
| Massive aggregates | 14.4 ± 1.7 | 24.0 ± 4.3[c] | 27.0 ± 6.4 | 20.5 ± 4.9 | 28.6 ± 5.2[c] | 16.3 ± 2.0 | 27.9 ± 7.4 | 28.5 ± 2.2[b] |
| Dot-like aggregates | 6.5 ± 1.4 | 8.7 ± 2.9 | 14.4 ± 1.5[a] | 39.7 ± 3.6[b] | 6.4 ± 0.7 | 33.5 ± 2.7[b] | 29.0 ± 5.8[a] | 17.1 ± 2.7[a] |
| (% of total γPKC-GFP expressing cells) | | | | | | | | |
| Phosphorylation level at | | | | | | | | |
| $Thr^{514}$ | 100 ± 4.4 | 68.5 ± 10.7 | 55.1 ± 5.4[a] | 26.2 ± 2.9[b] | 55.1 ± 2.4[b] | 88.0 ± 22.1 | 43.2 ± 3.4[b] | 29.6 ±8.0[a] |
| $Thr^{655}$ | 100 ± 8.7 | 74.4 ± 4.5 | 78.2 ± 13.9 | 53.5 ± 10.9[c] | 76.3 ± 4.9 | 84.0 ± 12.0 | 46.8 ± 7.6[a] | 65.5 ± 8.0[c] |
| $Thr^{674}$ | 100 ± 0.8 | 79.4 ± 3.2[a] | 70.3 ± 13.9 | 45.7 ± 6.8[a] | 59.1 ± 8.5[a] | 59.3 ± 12.5[c] | 37.7 ± 2.9[b] | 32.8 ± 8.2[a] |
| (% of WT) | | | | | | | | |
| Insolubility to | | | | | | | | |
| Triton X.100 | 60.6 ± 8.9 | 74.3 ± 6.7 | 82.7 ± 5.7 | 91.2 ± 2.6[c] | 52.1 ± 17.1 | 93.3 ± 1.7[c] | 94.3 ± 1.0[c] | 92.6 ± 1.7[c] |
| (% of expressed γPKC-GFP) | | | | | | | | |
| Translocation induced by ATP (1 mM) | | | | | | | | |
| Retained period at the plasma membrane (seconds) | 129.4 ± 23.2 | 114.4 ± 25.0 | 137.7 ± 9.3 | 95.0 ± 13.1[b] | 91.5 ± 8.1 | 123.3 ± 7.7 | 123.3 ± 9.1 | 117.5 ± 12.4 |
| Aggregation after the translocation (observed cells/examined cells) | 0/9 | 0/9 | 5/11 | 0/7 | 0/10 | 6/9[d] | 7/9[d] | 0/8 |
| Dead cells in | | | | | | | | |
| Total GFP(+) cells | 20.0 ± 0.8 | 20.3 ± 1.9 | 22.3 ± 1.3 | 31.5 ± 2.5[c] | 23.5 ± 1.5 | 25.5 ± 1.8[c] | 26.5 ± 2.5 | 25.5 ± 2.2 |
| Low GFP cells | 14.6 ± 0.2 | 11.7 ± 2.0 | 12.8 ± 1.3 | 17.1 ± 3.1 | 13.1 ± 1.9 | 14.6 ± 2.0 | 15.6 ± 2.5 | 15.9 ± 1.0 |
| High GFP cells | 32.2 ± 1.0 | 37.1 ± 1.6 | 40.9 ± 2.3[c] | 56.9 ± 0.9[b] | 52.7 ± 1.6[c] | 43.1 ± 4.2 | 47.1 ± 3.1[c] | 45.0 ± 3.2[c] |
| (% of GFP(+) cells) | | | | | | | | |

[a] $p < 0.01$.
[b] $p < 0.001$.
[c] $p < 0.05$ *versus* WT (unpaired *Student's t test*).
[d] $p < 0.01$ *versus* WT (Fisher's exact test).

complex marker (Fig. 4*A*). However, the massive aggregation of mutant γPKC-GFP was partially colocalized with WGA (Fig. 4*B*). This result indicates that massive aggregation of mutant γPKC-GFP was qualitatively different from that of wild type. In the case of dot-like aggregations, we could not establish colocalization of these aggregations with markers for Golgi complex, lysosome, or early or late endosomes (data not shown).

To elucidate whether γPKC-GFP irreversibly formed dot-like aggregates, we performed a FRAP study. A γPKC-GFP aggregation was photobleached with an argon laser at 488 nm, followed by observing fluorescence recovery. As shown in Fig. 5, an application of photobleaching into a circular area around dot-like aggregations (*a* and *b*) abolished the fluorescence of γPKC-GFP aggregation, and the GFP fluorescence was not recovered, at least within 30 min. In contrast, the fluorescence of non-aggregated γPKC-GFP (Fig, 5*c*) was recovered to a level similar to that in the unbleached cytoplasm within 1 min after photobleaching (Fig. 5*d*). This result indicates that mutant γPKC-GFP of dot-like aggregation tightly associates each other and that the aggregates were not exchangeable with free γPKC-GFP in the cytoplasm.

To exclude the possibility that the addition of GFP to the γPKC was critical for aggregate formation, we expressed mutant γPKC alone in CHO cells. We attempted to immunostain mutant γPKCs with anti-γPKC antibody. To confirm whether this antibody could properly detect the aggregation of γPKCs, CHO cells expressing mutant γPKC-GFP were stained with this antibody. As shown in Fig. 6*A*, the γPKC immunofluorescence detected with this antibody is consistent with the S119P γPKC-GFP fluorescence, although the antibody only recognized edges, not centers, of massive aggregations of S119P γPKC-GFP (*upper panels*, *arrows*). In contrast, the antibody recognized the whole of dot-like aggregations (*lower panels*, *arrowheads*). These results suggest that the anti-γPKC antibody properly recognizes γPKC-GFP aggregation, although it might be inaccessible to the centers of these aggregations. As shown in Fig. 6*B*, both massive (*arrow*) and dot-like (*arrowheads*) aggregations were also observed in CHO cells expressing S119P γPKC. In contrast, wild-type γPKC rarely aggregated in CHO cells (data not shown). This result indicates that the addition of GFP to γPKC is not critical for the aggregate formation of mutant γPKC.

*Phosphorylation Level and Solubility to Triton X-100 of Mutant γPKC-GFP Was Decreased*—γPKC has three phosphorylation sites in its kinase domain: activation loop ($Thr^{514}$), turn motif ($Thr^{655}$), and hydrophobic motif ($Thr^{674}$) site (Fig. 1). Phosphorylation of these three sites is necessary for the full activation of PKC in response to various stimulations (21–23). We examined whether the aggregate formation affected the phosphorylation level of these three sites by immunoblotting with each phosphospecific antibody. As shown in Fig. 7 and Table I, the phosphorylation levels of mutant γPKC-GFPs were significantly decreased or tended to be decreased at three phosphorylation sites, compared with those of wild type. Specifically, phosphorylation levels of three mutants (S119P, G128D, and F643L) were significantly lower at all three sites than those of wild type.

Various neurodegenerative diseases are accompanied by the formation of disease-specific inclusion bodies, for examples Lewy bodies in Parkinson disease, neurofibrillary tangles and senile plaques in Alzheimer disease, and nuclear inclusion bodies in Huntington disease (3, 24). These inclusion bodies are generated by aggregated, unfolded, or misfolded protein such as α-synuclein, tau, amyloid β-protein, and expanded polyglutamine, respectively. It has been reported that these unfolded or misfolded proteins became detergent-insoluble in cellular and animal models of various neurodegenerative diseases (25–27). Therefore, we examined whether mutated γPKC became insoluble to the detergent. Transfected CHO cells were separated into the 1% Triton-soluble (S) and -insoluble (I) fractions, and the amounts of γPKC-GFP in both fractions were quantified by immunoblotting with anti-GFP antibody. As shown in the upper panel of Fig. 8*A*, wild-type γPKC-GFP was detected with almost equal amounts in both S and I fractions. On the other hand,

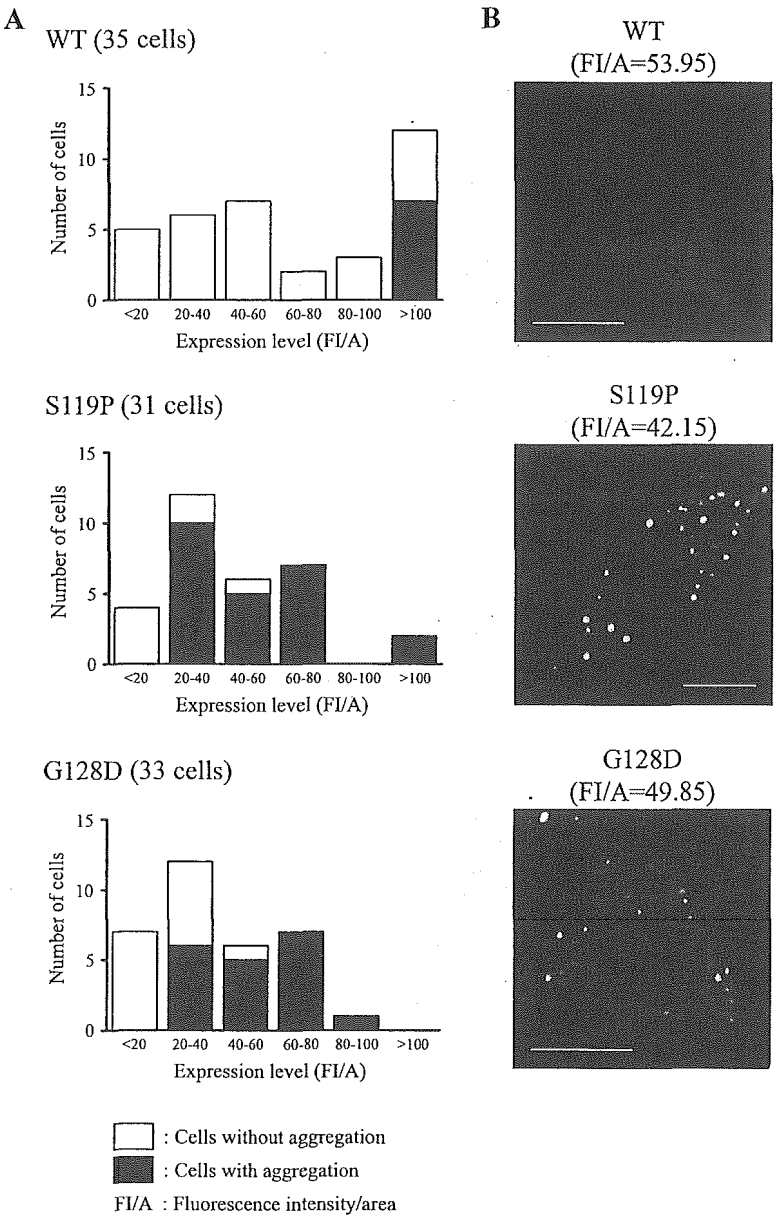


FIG. 3. **Relationship between expression level and aggregate formation of wild-type and mutant γPKC-GFPs (S119P and G128D).** *A*, histograms indicate the distribution of CHO cells expressing WT and S119P and G128D mutant γPKC-GFPs, which were classified into six groups according to their expression levels. The expression level was evaluated by the fluorescence intensity per area (FI/A) of each cell. *Closed* and *open bars* indicate the number of cells with and without aggregation, respectively. Total observed cells were 35, 31, and 33 cells in WT and S119P and G128D γPKC-GFPs, respectively. Cells were observed using confocal laser microscope 2 days after transfection. *B*, representative images of CHO cells expressing WT and S119P and G128D mutant γPKC-GFPs with FI/A 40–60. *Bar*, 10 μm.

mutant γPKC-GFPs were mostly detected in the I fraction. Especially, in S119P, Q127R, G128D, and F643L mutants, only faint bands were detected in the S fraction and very intense bands in I fraction. The amount of γPKC-GFP in the I fraction was quantified and indicated as percentage of the total fraction (Fig. 8*B* and Table I), which was used as an index of the insolubility to Triton X-100. Except in S119F, this value tended to increase, and significant differences were detected in S119P, Q127R, G128D, and F643L mutants compared with wild-type γPKC-GFP. This result suggests that mutant γPKC-GFPs became insoluble to 1% Triton X-100. The insolubilities of γPKC-GFPs to Triton X-100 were positively correlated ($r = 0.817$) with the extent of aggregated cells (Fig. 2*D*). For example, both values were high in S119P, Q127R, G128D, and F643L mutants and were relatively low in H101Y and S119F mutants. This correlation would imply that the insolubility of mutant γPKC-GFP to detergent was caused by its aggregated form.

Next, we compared the phosphorylation state of $Thr^{514}$ in the activation loop of γPKC, which is essential for PKC kinase activity (28, 29), between wild-type and mutant γPKC-GFP. The phosphorylation state was also compared between the S and I fractions. Phospho-$Thr^{514}$-specific antibody was used for assessment of the phosphorylation level (Fig. 8*A*, *lower panel*). γPKC-GFP in the S fraction was intensely phosphorylated. However, very few mutant γPKC-GFPs were phosphorylated in the I fraction although sufficient levels of mutant γPKC-GFP existed (Fig. 8*A*, *upper panel*). The relative phosphorylation level of $Thr^{514}$ per γPKC-GFP amount was shown in Fig. 8*C*. As for the S fraction, the phosphorylation level did not significantly differ between the wild-type and mutant γPKC-GFPs, although the phosphorylation level of S119F tended to be increased, compared with wild type. As for the I fraction, the phosphorylation level was obviously decreased in all wild-type and mutant γPKC-GFPs. These results suggest that mutant γPKC-GFPs in the S fraction were normally phosphorylated at $Thr^{514}$ to the same extent as the wild type. It is possible that γPKC-GFPs in the I fraction were mostly unphosphorylated at $The^{514}$ and inactive. As shown in Fig. 7, the phosphorylation levels of mutant γPKC-GFPs in RIPA-soluble total fraction were mostly decreased. This may be manifested because Triton-insoluble aggregated mutants were unphosphorylated.

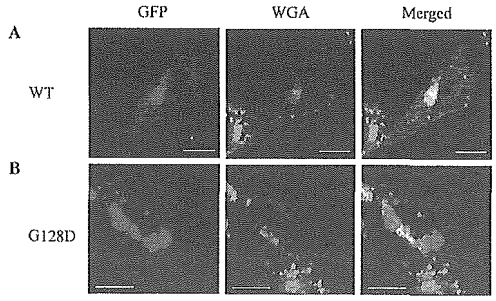


FIG. 4. **Alexa633-conjugated WGA, a marker of Golgi complex, was strongly colocalized with the massive aggregation of WT γPKC-GFP (*A*), but partially with that of G128D γPKC-GFP (*B*).** CHO cells expressing WT (*A*) and G128D (*B*) γPKC-GFP were fixed 2 days after transfection, followed by the staining with Alexa633-conjugated WGA to make the Golgi complex visible. The fluorescence of GFP and Alexa633 are shown in *green* (*left*) and *red* (*center*), respectively. In the merged image, the overlapping of GFP and Alexa633 signals appears *yellow* (*right*). *Bar*, 10 μm.

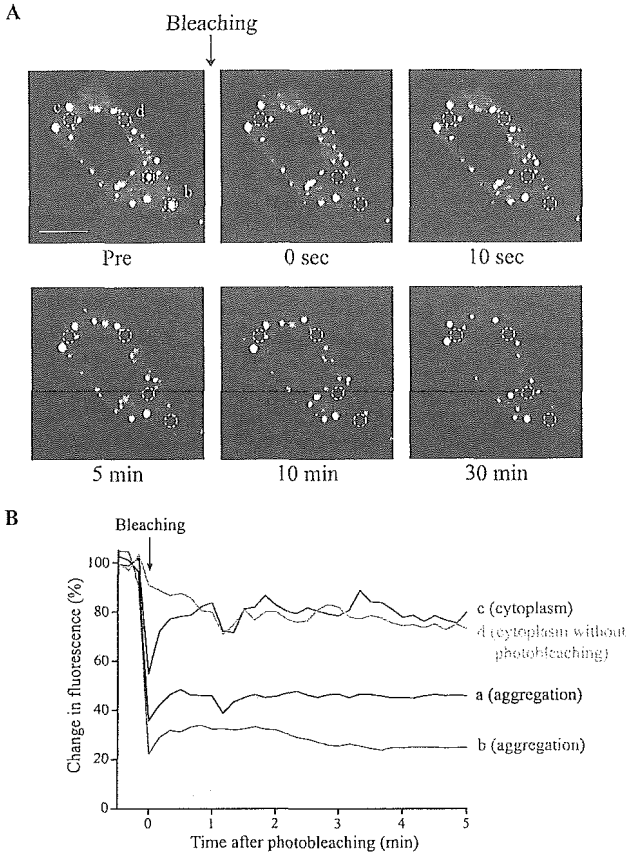


FIG. 5. **The fluorescence of γPKC-GFP was not recovered after photobleaching in a dot-like aggregation.** *A*, FRAP study was performed on cytoplasmic dot-like aggregation of γPKC-GFP. The images were obtained from CHO cells expressing S119P γPKC-GFP in every 10 s before and after the photobleaching. The images before (*upper left*) and 10 s (*upper center*) and 1, 5, 10, and 30 min (*upper right*, *lower left*, *lower center*, and *lower right*, respectively) after photobleaching are shown. *Circles* of *dotted lines* indicates bleached areas around dot-like aggregations (*a* and *b*), bleached areas in the cytoplasm without aggregation (*c*), and the unbleached area in the cytoplasm (*d*). *Bar*, 10 μm. *B*, time-dependent recoveries of fluorescence in the bleached areas (*a* and *b*, dot-like aggregations; *c*, cytoplasm without aggregation) and fading of fluorescence in the unbleached area (*d*) are shown as percentages of the fluorescence before photobleaching.

*Mutant γPKC-GFP Aggregated after Receptor-mediated Transient Translocation*—To examine whether receptor-mediated translocation of mutant γPKC-GFPs differed from that of

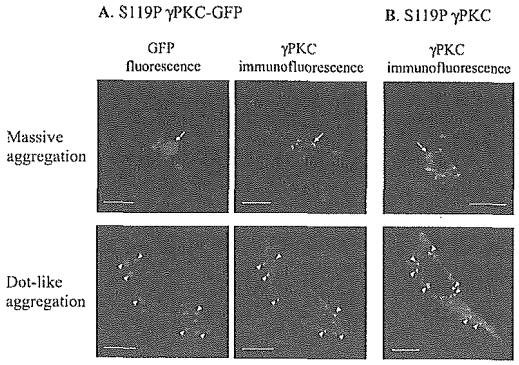


FIG. 6. **Fused GFP was not critical for aggregation of S119P γPKC-GFP.** Two days after transfection, CHO cells expressing S119P γPKC-GFP (*A*) and S119P γPKC (*B*) were fixed with 4% paraformaldehyde plus 0.2% picric acid and then immunostained with anti-γPKC antibody. Immunoreactivity was visualized with Alexa543-conjugated secondary antibody. The fluorescence of GFP and Alexa543 are shown in *green* (*left*) and *red* (*center*, *right*), respectively. *A*, anti-γPKC antibody recognizes both massive (*arrows* in *upper panels*) and dot-like (*arrowheads* in *lower panels*) aggregations of S119P γPKC-GFP although it only immunoreacts with the margin of massive aggregation. *B*, S119P γPKC alone forms both massive (*arrow*) and dot-like (*arrowheads*) aggregations, similar to S119P γPKC-GFP. *Bar*, 10 μm.

wild type, we observed the translocation of these γPKC-GFPs triggered by the stimulation of P2Y receptors, which are endogenously expressed in CHO cells (30). As reported previously (31), the application of ATP (1 mM) induced a rapid translocation of γPKC-GFP from the cytoplasm to the plasma membrane within 10 s after the stimulation, followed by a re-translocation from the membrane to cytoplasm around 2 min (Fig. 9*A*). Likewise, all mutant γPKC-GFPs were transiently translocated from cytoplasm to the plasma membrane in CHO cells without any aggregations (Fig. 9). The translocation of mutant γPKC-GFP occurred within 10 s after the stimulation, and there were no differences in the retention period at the plasma membrane between wild-type and mutants (Table I).

However, in many cells expressing G118D, Q127R, and G128D, γPKC-GFP formed punctuate aggregates in the cytoplasm after the reversion from plasma membrane to cytoplasm (Fig. 9*C* and Supplemental Video). In these cells, mutant γPKC-GFP behaved in a similar manner to wild type until 2 min after the stimulation. Thereafter, γPKC-GFP started to aggregate in the cytoplasm and almost all γPKC-GFP in the cytoplasm aggregated within 10 min (Fig. 9*C* and Supplemental Video). These phenomena were seen in 45, 67, and 78% of cells expressing G118D, Q127R, and G128D, respectively, to which translocation studies were applied (Table I). These results suggest that the aggregate formation of mutant γPKC-GFP was frequently triggered by its receptor-mediated translocation.

As is shown in Fig. 2, in some cells, aggregation had already observed before the stimulation. In these cells, diffusely expressed cytoplasmic γPKC-GFP was translocated, but aggregated γPKC-GFP was not (data not shown).

*Mutant γPKC-GFP Induced Cell Death in Parallel with Its Expression Level*—Overexpression of etiological gene products has been reported to cause cell death in cellular and animal models of various neurodegenerative diseases (5, 32, 33). We investigated whether these mutant γPKC-GFPs caused cell death. Three days after transfection of wild-type or mutant γPKC-GFPs, CHO cells were stained with 7-AAD, a fluorescent DNA dye that selectively enters dead cells (34). Stained cells were applied to flow cytometry and were classified by two parameters, GFP and 7-AAD fluorescence. Representative results using wild type and S119P are shown in Fig. 10, *A* and *B*, respectively. The GFP and 7-AAD fluorescence of each cell was

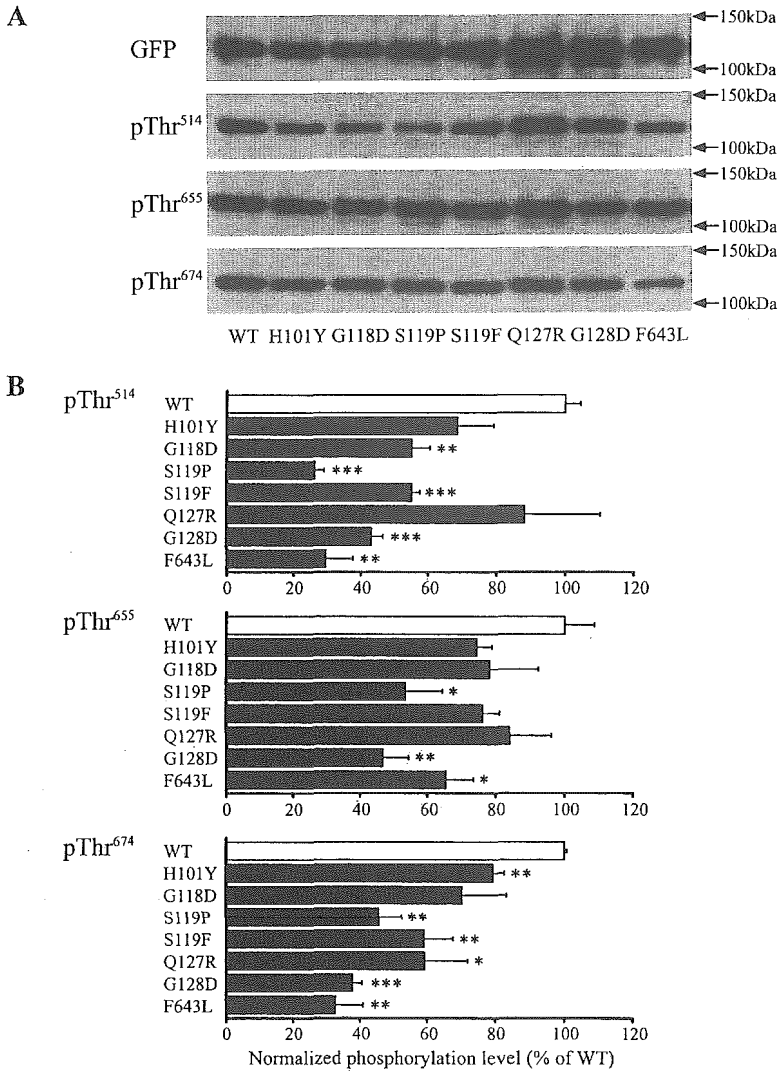


FIG. 7. **Mutant γPKC-GFPs had less phosphorylation at their three phosphorylation sites.** *A*, immunoblotting analysis of WT and mutant γPKC-GFPs with anti-GFP and anti-phosphorylated threonine (pThr$^{514}$, pThr$^{655}$, and pThr$^{673}$) -specific antibodies. Protein samples were extracted from CHO cells 2 days after transfection. Total fraction of each sample (10 μg of protein) was subjected to 7.5% SDS-PAGE, followed by immunoblotting. Data shown are representative of three experiments. *B*, normalized phosphorylation level at each threonine residue. Chemiluminescence of immunoreactive bands were quantified using Fluor-S MultiImager. In each sample, the intensity of band detected with a phosphospecific antibody was normalized by that detected with anti-GFP antibody. Data are presented as percentages of normalized value in WT. *, $p < 0.05$; **, $p < 0.01$; ***, $p < 0.001$ *versus* WT (unpaired Student's *t* test, $n = 3$).

positioned as a dot in the graph. Cells in the right lower part (GFP(+)/7-AAD(−)) represented viable cells expressing γPKC-GFPs, and cells in the right upper part (GFP(+)/7-AAD(+)) represented dead cells expressing γPKC-GFPs. The GFP-positive cells expressing S119P γPKC-GFP were better stained with 7-AAD than cells expressing wild-type γPKC-GFP (Fig. 10, *A* and *B*). The percentages of dead cells in total GFP-positive cells were shown in Fig. 10*C*. In CHO cells expressing S119P and Q127R mutant γPKC-GFPs, the percentages of dead cells were significantly higher (31.5 ± 2.5 and 25.5 ± 1.8%, respectively) than that in cells expressing wild type (20.0 ± 0.8%). To evaluate whether the expression level of γPKC-GFP affects the cell viability, GFP-positive cells were divided into two groups: groups with low and high GFP fluorescence (low and high GFP group, Fig. 10*B*), and the percentages of dead cells were calculated in each group. In the low GFP group, there were no significant differences in cell viabilities between wild-type and mutant γPKC-GFP-expressing cells (Fig. 10*D*). However, in the high GFP group, cytotoxic effects of mutant γPKC-GFPs were more prominently manifested than in total GFP-positive cells (Fig. 10*E*). G118D, S119P, S119F, and G128D significantly exacerbated cell death, compared with wild type. In addition, H101Y and Q127R mutants tended to cause cell death more prominently than wild type. These results suggest that mutant γPKC-GFP induced cell death in parallel with its expression level.

## DISCUSSION

Several autosomal dominant SCAs have been revealed to be caused by abnormal expansions of CAG trinucleotide repeats (1, 2). In these polyglutamine diseases, expanded polyglutamine chains can easily form β-sheet structures and insoluble aggregates in the neuronal cells (3, 4). Similar insoluble aggregations of mutant or misfolded proteins are frequently observed in various inherited neurodegenerative disorders including Alzheimer disease and Parkinson disease (3, 24, 35). The gain of toxic function derived from aggregated mutant proteins is considered to be the etiology of these late-onset neurodegenerative disorders. In the present study, we demonstrated that missense mutations of the *γPKC* gene, found in SCA14, induced the formation of insoluble γPKC aggregates and cell death in CHO cells.

Two types of aggregation, massive and dot-like aggregations were frequently observed in CHO cells expressing mutant γPKC-GFP (Fig. 2). Dot-like aggregations, frequently shown in CHO cells expressing S119P, Q127R, and G128D mutants, might be caused by the accumulation of γPKC-GFP to cellular organelles such as lysosome or endosomes. However, we could not clearly find the colocalization of this aggregation with any organelles (data not shown). Moreover, FRAP analysis confirmed that γPKC-GFP in these aggregations was tightly associated and not exchangeable with free γPKC-GFP in the cyto-

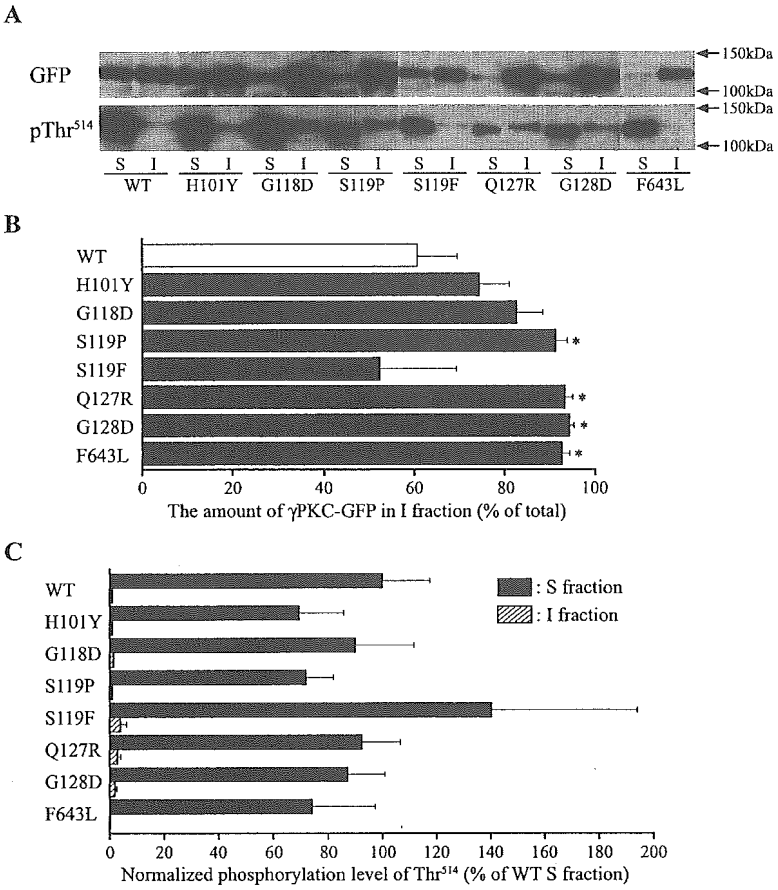


FIG. 8. **Mutant γPKC-GFPs were insoluble to Triton X-100 and were markedly less phosphorylated at Thr$^{514}$ in the Triton-insoluble fraction.** *A*, immunoblotting analysis of Triton-soluble (*S*) and Triton-insoluble (*I*) fractions, which were prepared from CHO cells expressing WT and mutant γPKC-GFPs, was performed using anti-GFP and anti-phosphorylated Thr$^{514}$ (pThr$^{514}$) -specific antibodies. Two days after transfection, CHO cells were harvested and separated into S and I fractions as described in the text. Five percent of each fraction was subjected to 7.5% SDS-PAGE, followed by immunoblotting. Data shown are representative of four experiments. *B*, insolubility of WT and mutant γPKC-GFP to Triton X-100. The amount of γPKC-GFPs in each fraction was quantified by the band intensity detected with anti-GFP antibody. The amount of γPKC-GFP in the I fraction is presented as the percentage of that in the total fraction (S plus I fraction). This value was used as an index showing insolubility to Triton X-100. *, $p < 0.05$ *versus* WT (unpaired Student's *t* test, WT; $n = 8$, mutant; $n = 4$). *C*, normalized phosphorylation level at Thr$^{514}$ in S and I fractions. The intensity of immunoreactive band detected with anti-phosphorylated Thr$^{514}$ antibody was normalized by that detected with anti-GFP antibody. This value was used as the phosphorylation level at Thr$^{514}$ in each sample. Data are presented as percentages of phosphorylation levels at Thr$^{514}$ in the S fraction of WT. *Black* and *hatched bars* represent the phosphorylation level at Thr$^{514}$ in the S and I fraction, respectively.

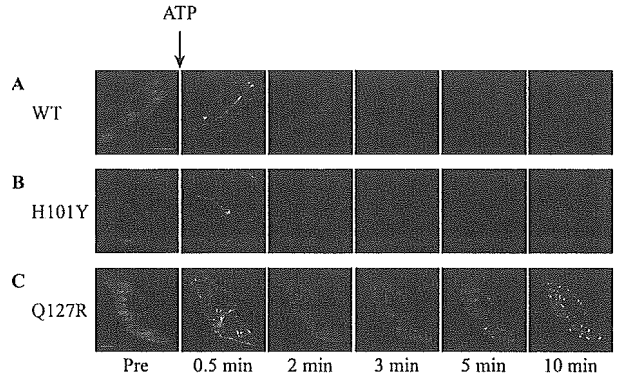


FIG. 9. **Several mutant γPKC-GFPs formed cytoplasmic dot-like aggregates after its receptor-mediated transient translocation.** CHO cells expressing wild type (*A*), H101Y (*B*), and Q127R (*C*) mutant γPKC-GFPs were stimulated with ATP (1 mM), an agonist of P2Y receptor. The sequential changes in the fluorescence of GFP fusion protein were monitored. Images before (*pre*) and 0.5, 2, 3, 5, and 10 min after ATP stimulation are shown. ATP induced transient γPKC-GFP translocation from the cytoplasm to the plasma membrane in CHO cells expressing both wild-type and mutant γPKC-GFPs. Q127R γPKC-GFP gradually aggregated in a dot-like manner after re-translocation to cytoplasm (3, 5, 10 min in *C*). Data shown are representative of at least five experiments. *Bar* = 10 μm. Live imaging of Q127RγPKC-GFP translocation can be seen in a Supplemental Video.

plasm (Fig. 5). This result is consistent with previous reports that the GFP fluorescence of polyglutamine protein aggregates is not recovered after photobleaching (36, 37). These findings indicate that dot-like accumulations of mutant γPKC-GFP are indeed aggregates, but are not the simple result of targeting to particular cell organelles.

Massive aggregations, frequently shown in cells expressing H101Y, G118D, S119F, and F643L mutants, were located near the nucleus, but partially localized to Golgi complex, whereas massive aggregations of wild type showed strong colocalization with the Golgi complex (Fig. 4). This result might imply that the mechanism of massive-aggregate formation of mutant γPKC-GFPs was different from that of wild type. The long term time-lapse imaging of mutant γPKC-GFP aggregation is necessary to elucidate how massive aggregations are formed.

In seven missense mutations examined in the present study, six mutations were located around the C1B domain (Fig. 1), which is involved in the binding to various lipid messengers like DG (17–19). These mutations might affect the lipid binding, resulting in the aggregate formation.

Both wild-type and mutant γPKC-GFPs were transiently translocated from cytoplasm to plasma membrane in CHO cells by P2Y receptor stimulation with ATP (Fig. 9). No significant differences were found in parameters of PKC translocation, such as translocation or re-translocation speed and PKC-retaining periods at plasma membrane, between wild type and mutants (Table I). It suggests that the six missense mutations around C1B domain did not robustly affect the properties of receptor-mediated PKC translocation. This is inconsistent with results reported by Verbeek *et al.* (38), showing that calcium ionophore-induced translocation was hastened in two mutant γPKC-GFPs found in SCA14 families; one is G118D and the other is C150F, a newly found missense mutation. This discrepancy may be explained by the difference in stimulation and cell types; however, it is still controversial whether mutations affect the PKC regulation mechanism and subsequently alter its translocation.

Although the translocation process of mutant PKC is likely similar to that of wild type, three mutant (G118D, Q127R, and G128D) γPKC-GFPs rapidly and irreversibly aggregated in the cytoplasm after the receptor-mediated translocation (Fig. 9*C*

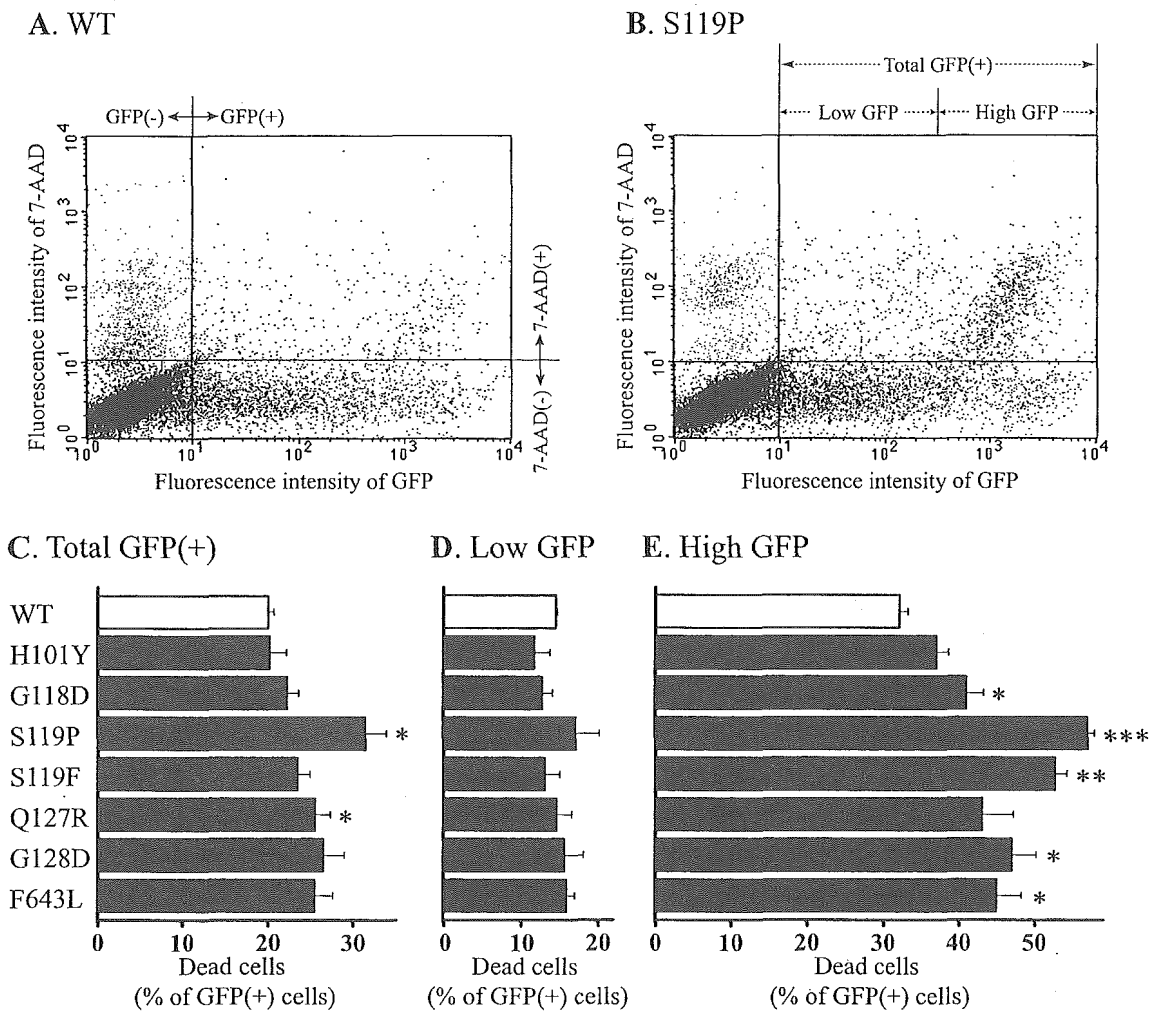


FIG. 10. **Flow cytometric analysis of cell death in CHO cells expressing wild-type and mutant γPKC-GFPs.** Transfected cells were cultured for 3 days and then stained with 7-AAD, a dye targeting dead cells. Stained cells were separated by two dimensions, GFP and 7-AAD fluorescence using flow cytometry. *A* and *B*, representative GFP/7-AAD dot plots of CHO cells expressing wild type (*A*) and S119P (*B*) mutant γPKC-GFPs. Cells in *right upper* and *lower quadrants* (GFP(+) in *A*) were considered to express γPKC-GFP. Cells in *upper right* and *left quadrants* (7-AAD(+) in *A*) were considered to be dead. *C–E*, percentages of dead cells in GFP-positive CHO cells expressing WT and mutant γPKC-GFPs analyzed by flow cytometry. The results of total GFP(+) cells were shown in *C*. Total GFP(+) cells were divided into two groups, cells with low and high GFP fluorescence (*Low GFP* and *High GFP*, respectively). The percentages of dead cells in low and high GFP groups are shown in *D* and *E*, respectively. *, $p < 0.05$; **, $p < 0.01$ *versus* WT (unpaired Student's *t* test, $n = 3$).

and Supplemental Video). The aggregation pattern resembled the dot-like aggregation (Fig. 2*C*) although we did not confirm whether these two types of aggregation were identical. When the stimulation of $G_q$-protein-coupled receptors translocate PKC to the plasma membrane, PKC interacts with its activator, diacylglycerol and $Ca^{2+}$, which are elevated by the stimulation It is well accepted that this interaction triggers the conformational change of the PKC molecule and allows PKC to be active (21, 39). This conformational change of mutant γPKC-GFP might cause the rapid aggregation of γPKC-GFP. In unstimulated CHO cells, the endogenous receptor activation might trigger the translocation, activation, conformational change, and aggregation of mutant γPKC-GFP during proliferation of CHO cells. The dot-like aggregation might be formed by repetitive endogenous receptor activation.

In the present study, Triton-insoluble γPKC-GFP seemed to be inactive because it was marginally phosphorylated at $Thr^{514}$ in the activation loop (Fig. 8, *C* and *D*), which is phosphorylated by PDK1 and is most essential for kinase activity in the three main phosphorylation sites of γPKC ($Thr^{514}$, $Thr^{655}$, and $Thr^{674}$) (21–23, 28, 29, 40, 41) (Fig. 1). Because the insolubility of γPKC-GFPs to Triton X-100 were positively correlated ($r$ = 0.817) with the extent of its aggregation, this result would imply that aggregated γPKC-GFP was unphosphorylated and inactive. This raises the possibility that the reduction of γPKC function, caused by the aggregate formation, is the etiology of SCA14. Indeed, γPKC knock-out mice showed mildly impaired motor coordination and mild deficits in spatial and contextual learning (12, 42), similar pathologies observed in SCA14. However, these symptoms seemed to be more severe in SCA14 patients than in knock-out mice although mutations found in SCA 14 are heterozygous, leading to the idea that the gain of toxic function, not the loss of γPKC function derived from mutant γPKC, would trigger various cerebellar symptoms.

In the recent study reported by Verbeek *et al.* (38) the increase of basal kinase activity was observed in G118D and C150F mutant γPKC-GFPs. They also demonstrated that these mutant γPKC-GFPs had similar phosphorylation levels at three sites to wild-type γPKC-GFP. These findings appear to conflict with our findings. This discrepancy is interpreted by the difference in the timing of observation. In the present study, our experiments were conducted 2 or 3 days after transfection, whereas Verbeek *et al.* observed the phosphorylation and kinase activity 24 h after transfection. We confirmed that

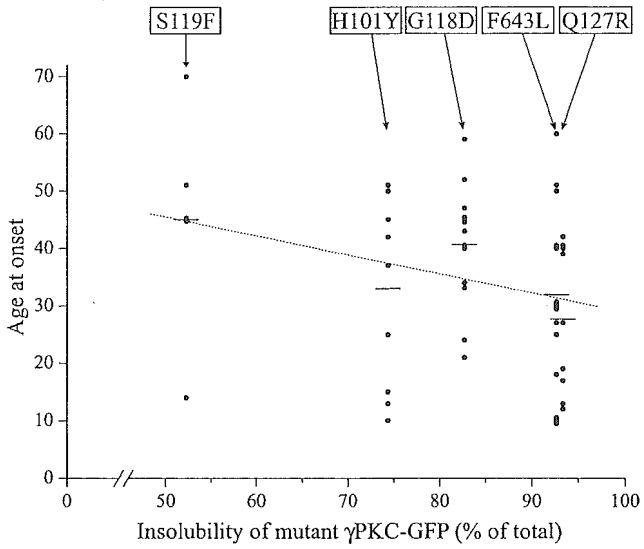


FIG. 11. **The insolubility of mutant γPKC-GFP is negatively correlated with age at onset of affected patients in SCA14 families.** The dot plot shows the relationship between the insolubility of each mutant γPKC-GFP, shown in Fig. 6*B*, and the distribution of ages at onset in the corresponding SCA14 family. A missense mutation of γPKC in each family is shown in the *box*. We analyzed five families (H101Y, G118D, S119F, Q127R, and F643L) where more than five patients were reported to be affected. The *bar* in each family represents the average age at onset. The *dotted line* indicates the negative correlation between the insolubility to Triton X-100 and the average age at onset ($r = -0.811$).

lower aggregation and lower insolubility to Triton X-100 of mutant γPKC-GFPs were observed 1 day after transfection in our experiments (data not shown). Furthermore, our preliminary study demonstrated that the basal kinase activities were not increased in all of the SCA14 γPKC mutants, although we confirmed the increased basal activity of G118D.[2] This result suggests that the elevated basal activity found in G118D could not simply account for the whole aspect of SCA14 pathogenesis.

Our present study demonstrated that the susceptibility to aggregate formation and solubility to Triton X-100 varied among mutant γPKC-GFPs found in several SCA14 families (Figs. 2 and 7). To explore whether these variations are correlated with the clinical features of each SCA14 family, we investigated the relationship between the Triton solubility of mutant γPKC-GFPs and average age at onset of ataxia in five SCA families (H101Y, G118D, S119F, Q127R, and F643L) in which more than five persons were reported to be affected. As shown in Fig. 11, the average onset age of each family is negatively correlated with the insolubility of the corresponding γPKC mutant ($r = -0.8115$). This strongly suggests that insoluble γPKC formed by the missense mutation is implicated in the pathogenesis of SCA14.

Although the formation of insoluble aggregation is thought to exert neurotoxic effects in several inherited neurodegenerative diseases (3, 24), the precise molecular mechanism is uncertain. The ubiquitin-proteasome system (UPS) is one of the major proteolytic pathways in mammalian cells that is involved in the degradation of cytosolic short-lived proteins (43). The UPS is also involved in the elimination system of inappropriate folded proteins, which prevents them from aggregating. Age-related decline of UPS function results in the increased accumulation and aggregation of misfolded proteins. Protein aggregation further exacerbates UPS dysfunction by sequestrating the 26 S proteasome complex into the aggregation (44). This is the commonly accepted mechanism of neuronal cell death in neurodegenerative diseases accompanying protein aggregation (44–46). In our preliminary experiments, increased ubiquitination was found in several mutant γPKC-GFPs. Although further studies are necessary to elucidate the involvement of UPS in SCA14 pathogenesis, it is plausible that mutant γPKC aggregation exerts its cytotoxic effects on neurons by disturbing the UPS.

In various neurodegenerative diseases, the disease-specific inclusion bodies, for example Lewy bodies in Parkinson disease, neurofibrillary tangles and senile plaques in Alzheimer disease, and nuclear inclusion bodies in Huntington disease (3, 24) were observed. However, the autopsy report from the SCA14 patient having the H101Y mutation revealed no aggregation of γPKC in the cerebellar neurons (6). At present, we do not have adequate answers to explain why the mutant γPKC does not form aggregates in the Purkinje cells of actual SCA14 patients. Further autopsy studies from specimens with mutations other than H101Y are necessary to resolve the discrepancy because the H101Y mutant had the lowest tendency to aggregate among the mutant PKC-GFP examined in the present study (Fig. 2*D* and Table I).

The findings in the present study provide the possibility that SCA14 is caused by a mechanism similar to other neurodegenerative diseases; that is the accumulation of aggregated protein. Although further studies are necessary to identify the precise molecular mechanism of mutant γPKC to cause SCA14, the identification may lead to effective therapeutic methods not only for SCA14 but also for other neurodegenerative diseases.

*Acknowledgment*—This work was carried out with equipment from the Analysis Center of Life Science, Hiroshima University.

REFERENCES

1. Mariotti, C., and Di Donato, S. (2001) *Neurol. Sci.* **22,** Suppl. 2, S88–S92
2. Schols, L., Bauer, P., Schmidt, T., Schulte, T., and Riess, O. (2004) *Lancet Neurol.* **3,** 291–304
3. Martin, J. B. (1999) *N. Engl. J. Med.* **340,** 1970–1980
4. Everett, C. M., and Wood, N. W. (2004) *Brain* **127,** 2385–2405
5. Ikeda, H., Yamaguchi, M., Sugai, S., Aze, Y., Narumiya, S., and Kakizuka, A. (1996) *Nat. Genet.* **13,** 196–202
6. Chen, D. H., Brkanac, Z., Verlinde, C. L., Tan, X. J., Bylenok, L., Nochlin, D., Matsushita, M., Lipe, H., Wolff, J., Fernandez, M., Cimino, P. J., Bird, T. D., and Raskind, W. H. (2003) *Am. J. Hum. Genet.* **72,** 839–849
7. van de Warrenburg, B. P., Verbeek, D. S., Piersma, S. J., Hennekam, F. A., Pearson, P. L., Knoers, N. V., Kremer, H. P., and Sinke, R. J. (2003) *Neurology* **61,** 1760–1765
8. Yabe, I., Sasaki, H., Chen, D. H., Raskind, W. H., Bird, T. D., Yamashita, I., Tsuji, S., Kikuchi, S., and Tashiro, K. (2003) *Arch. Neurol.* **60,** 1749–1751
9. Stevanin, G., Hahn, V., Lohmann, E., Bouslam, N., Gouttard, M., Soumphonphakdy, C., Welter, M. L., Ollagnon-Roman, E., Lemainque, A., Ruberg, M., Brice, A., and Durr, A. (2004) *Arch. Neurol.* **61,** 1242–1248
10. Saito, N., Kikkawa, U., Nishizuka, Y., and Tanaka, C. (1988) *J. Neurosci.* **8,** 369–382
11. Saito, N., and Shirai, Y. (2002) *J. Biochem. (Tokyo)* **132,** 683–687
12. Chen, C., Kano, M., Abeliovich, A., Chen, L., Bao, S., Kim, J. J., Hashimoto, K., Thompson, R. F., and Tonegawa, S. (1995) *Cell* **83,** 1233–1242
13. Kano, M., Hashimoto, K., Chen, C., Abeliovich, A., Aiba, A., Kurihara, H., Watanabe, M., Inoue, Y., and Tonegawa, S. (1995) *Cell* **83,** 1223–1231
14. Skinner, P. J., Vierra-Green, C. A., Clark, H. B., Zoghbi, H. Y., and Orr, H. T. (2001) *Am. J. Pathol.* **159,** 905–913
15. Sakai, N., Tsubokawa, H., Matsuzaki, M., Kajimoto, T., Takahashi, E., Ren, Y., Ohmori, S., Shirai, Y., Matsubayashi, H., Chen, J., Duman, R. S., Kasai, H., and Saito, N. (2004) *Genes Cells* **9,** 945–957
16. Nishizuka, Y. (1995) *FASEB J.* **9,** 484–496
17. Nishizuka, Y. (1986) *Science* **233,** 305–312
18. Ono, Y., Fujii, T., Igarashi, K., Kuno, T., Tanaka, C., Kikkawa, U., and Nishizuka, Y. (1989) *Proc. Natl. Acad. Sci. U. S. A.* **86,** 4868–4871
19. Irie, K., Nakahara, A., Nakagawa, Y., Ohigashi, H., Shindo, M., Fukuda, H., Konishi, H., Kikkawa, U., Kashiwagi, K., and Saito, N. (2002) *Pharmacol. Ther.* **93,** 271–281
20. Cho, W. (2001) *J. Biol. Chem.* **276,** 32407–32410
21. Hofmann, J. (1997) *FASEB J.* **11,** 649–669
22. Parekh, D. B., Ziegler, W., and Parker, P. J. (2000) *EMBO J.* **19,** 496–503
23. Newton, A. C. (2003) *Biochem. J.* **370,** 361–371
24. Johnson, W. G. (2000) *J. Anat.* **196,** 609–616
25. Waelter, S., Boeddrich, A., Lurz, R., Scherzinger, E., Lueder, G., Lehrach, H., and Wanker, E. E. (2001) *Mol. Biol. Cell* **12,** 1393–1407
26. DeTure, M., Ko, L. W., Easson, C., and Yen, S. H. (2002) *Am. J. Pathol.* **161,** 1711–1722
27. Klucken, J., Shin, Y., Masliah, E., Hyman, B. T., and McLean, P. J. (2004) *J. Biol. Chem.* **279,** 25497–25502
28. Cazaubon, S., Bornancin, F., and Parker, P. J. (1994) *Biochem. J.* **301,** 443–448

29. Orr, J. W., and Newton, A. C. (1994) *J. Biol. Chem.* **269,** 27715–27718
30. Iredale, P. A., and Hill, S. J. (1993) *Br. J. Pharmacol.* **110,** 1305–1310
31. Shirai, Y., Sakai, N., and Saito, N. (1998) *Jpn. J. Pharmacol.* **78,** 411–417
32. Giasson, B. I., Duda, J. E., Quinn, S. M., Zhang, B., Trojanowski, J. Q., and Lee, V. M. (2002) *Neuron* **34,** 521–533
33. Zhou, W., and Freed, C. R. (2004) *J. Biol. Chem.* **279,** 10128–10135
34. Schmid, I., Krall, W. J., Uittenbogaart, C. H., Braun, J., and Giorgi, J. V. (1992) *Cytometry* **13,** 204–208
35. Ross, C. A., and Poirier, M. A. (2004) *Nat. Med.* **10,** (suppl.) S10–S17
36. Chai, Y., Shao, J., Miller, V. M., Williams, A., and Paulson, H. L. (2002) *Proc. Natl. Acad. Sci. U. S. A.* **99,** 9310–9315
37. Kim, S., Nollen, E. A., Kitagawa, K., Bindokas, V. P., and Morimoto, R. I. (2002) *Nat. Cell Biol.* **4,** 826–831
38. Verbeek, D. S., Knight, M. A., Harmison, G. G., Fischbeck, K. H., and Howell, B. W. (2005) *Brain* **128,** 436–442
39. Newton, A. C. (1997) *Curr. Opin. Cell Biol.* **9,** 161–167
40. Le Good, J. A., Ziegler, W. H., Parekh, D. B., Alessi, D. R., Cohen, P., and Parker, P. J. (1998) *Science* **281,** 2042–2045
41. Dutil, E. M., Toker, A., and Newton, A. C. (1998) *Curr. Biol.* **8,** 1366–1375
42. Abeliovich, A., Paylor, R., Chen, C., Kim, J. J., Wehner, J. M., and Tonegawa, S. (1993) *Cell* **75,** 1263–1271
43. Hershko, A., and Ciechanover, A. (1998) *Annu. Rev. Biochem.* **67,** 425–479
44. Chai, Y., Koppenhafer, S. L., Shoesmith, S. J., Perez, M. K., and Paulson, H. L. (1999) *Hum. Mol. Genet.* **8,** 673–682
45. Bence, N. F., Sampat, R. M., and Kopito, R. R. (2001) *Science* **292,** 1552–1555
46. Cummings, C. J., Reinstein, E., Sun, Y., Antalffy, B., Jiang, Y., Ciechanover, A., Orr, H. T., Beaudet, A. L., and Zoghbi, H. Y. (1999) *Neuron* **24,** 879–892

Guidelines for the Management of Stroke 2004. (in Japanese) Kyowa-kikaku, Tokyo, 2004.
7) Astrup J, Siesjo BK, Symon L. Thresholds in cerebral ischemia—the ischemic penumbra. stroke **12**: 723–725, 1981.
8) Heiss WD. Experimental evidence for ischemic thresholds and functional recovery. Stroke **23**: 1668–1672, 1992.
9) Hacke W, Kaste M, Fieschi C, et al. Intravenous thrombolysis with recombinant tissue plasminogen activator for acute hemispheric stroke. The European Cooperative Acute Stroke Study (ECASS). JAMA **274**: 1017–1025, 1995.
10) Hacke W, Kaste M, Fieschi C, et al. Randomised double-blind placebocontrolled trial of thrombolytic therapy with intravenous alteplase in acute ischemic stroke (ECASS II). Second European-Australian Acute Stroke Study Investigators. Lancet **352**: 1245–1251, 1998.
11) Fagan SC, Morgenstern LB, Petitta A, et al. Cost-effectiveness of tissue plasminogen activator for acute ischemic stroke. NINDS rt-PA Stroke Study Group. Neurology **50**: 883–890, 1998.
12) Kwiatkowski TG, Libma RB, Frankel M, et al. Effects of tissue plasminogen activator for acute ischemic stroke at one year. National Institute of Neurological Disorders and Stroke Recombinant tissue Pasminogen Activator Stroke Study Group. N Engl J Med **340**: 1781–1787, 1999.
13) Furlan A, Higashida R, Wechsler L, et al. Intra-arterial prourokinase for acute ischemic stroke. The PROACT II Study: A randomized controlled trial. Prolyse in Acute Cerebral thromboembolism. JAMA **282**: 2003–2011, 1999.
14) Chiu D, Krieger D, Villar-Cordova C, et al. Intravenous tissue plasminogen activator for acute ischemic stroke. Feasibility, safety, and efficacy in the first year of clinical practice. Stroke **29**: 18–22, 1998.
15) Grotta JC. Acute stroke therapy at the millennium: Consummating the marriage between the laboratory and bedside. The Feinberg Lecture. Stroke **30**: 1722–1728, 1999.
16) Katzan IL, Furlan AJ, Lloyd LE, et al. Use of tissue-type plasminogen activator for acute ischemic stroke: The Cleveland area experience. JAMA **283**: 1151–1158, 2000.
17) Yamaguchi T. Acute stroke management in Japan: present and future perspective. Jpn J Stroke **23**: 261–268, 2001 (in Japanese with English Abstract).

# 5. Future Aspects of Gene Therapy in Acute Ischemic Stroke

Kazuo KITAGAWA, Masatsugu HORI and Masayasu MATSUMOTO*

Department of Internal Medicine and Therapeutics, Osaka University Graduate School of Medicine, Osaka
and *Department of Clinical Neuroscience, Hiroshima University Graduate School of Biomedical Sciences, Hiroshima

***Key words:*** gene therapy, brain ischemia, macrophage, neurogenesis

Neural stem/progenitor cells remain in the adult mammalian brain, including the human brain. Neurogenesis continues throughout life in the two restricted zones, the hippocampal subgranular zone (SGZ) and the rostral migratory stream, where newly generated immature neurons migrate from the anterior subventricular zone (SVZ) into the olfactory bulb. Brain injury including ischemia stimulates neurogenesis in the SGZ and SVZ (1, 2). Therefore, therapeutic strategy for enhancing neurogenesis after ischemia may be of value for promoting functional recovery in stroke patients with neurological deficits. Intracerebral or intraventricular injections of neurotrophic factors could stimulate neurogenesis in the ischemic hippocampus and caudoputamen (3, 4). However, dependence on invasive surgical procedures for delivery could limit clinical application (Fig. 1A, B). Therefore, non-invasive, safe, and inexpensive strategies would be required for clinical application for enhancing neurogenesis in stroke patients. Several previous studies including our own have demonstrated that circulating monocytes or macrophages begin to infiltrate ischemic tissue after infarction develops (5). Peripheral blood mononuclear cells and macrophages have drawn much attention as novel cellular vehicles for gene therapies in which these cells are genetically modified *ex vivo* and then reintroduced into the body (6). Furthermore, cationic liposome/DNA complexes have been shown to be capable of transfecting monocytes/macrophages *in vivo* in blood, liver, and spleen (7). These observations suggest that after systemic intravenous injection of a cationic liposome/DNA complex, circulating monocytes/macrophages could take up the introduced gene and infiltrate infarcted tissue. Therefore we tried to develop the systemic gene therapy using infiltrating macrophages as cell vehicles. We used an enhanced green fluorescent protein (EGFP) expression vector complexed with cationic liposomes for systemic gene therapy. After systemic administration of pIRES-EGFP plasmid vector with Lipofectin into normal rats, no EGFP-positive cells or macrophages were observed in intact brain. However, macrophages markedly accumulated in the brain tissue once infarct developed (Fig. 1C), and large numbers of EGFP-positive cells were detected in the marginal zone of the infarct. Expression of the exogenous EGFP gene was

Reprint requests should be addressed to Dr. Kazuo Kitagawa, Division of Stroke Research, Department of Internal Medicine and Therapeutics (A8), Osaka University Graduate School of Medicine, 2-2 Yamada-oka, Suita, Osaka 565-0871

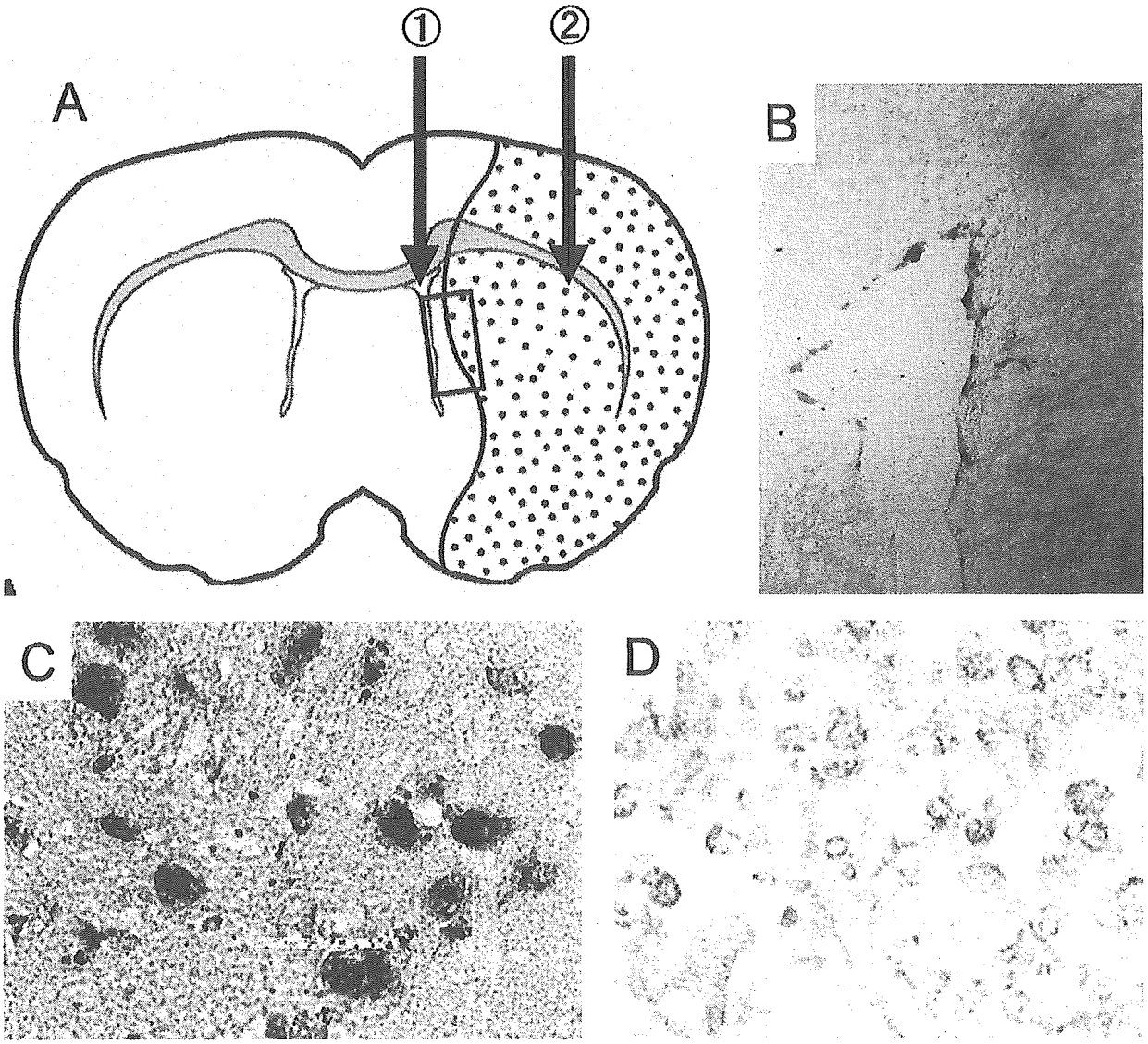


**Figure 1. The diagram depicts sections of the rat brain after middle cerebral artery (MCA) occlusion with the infarct shown as stippled (A). The border area is indicated by the rectangular box in the striatum. Intraventricular (1) or intracerebral (2) injection is widely used for gene transfer into the brain. Intraventricular administration of adenoviral reporter gene resulted in expression of exogenous gene on the wall of the lateral ventricule (B). Macrophages accumulating along the margin of the evolving infarct are shown with anti-Mac2 antibody in (C). Immunohistochemistry with anti-EGFP antibody was used to confirm EGFP protein expression in the ischemic caudoputamen after intravenous injection of pIRES-EGFP plasmid vector (D).**

confirmed immunohistochemically using an anti-EGFP antibody (Fig. 1D). Most EGFP-positive cells expressed monocyte/macrophage specific antigens. To deliver exogenous FGF-2 gene to the infarct, we injected pIRES-FGF2-EGFP plasmid. Marked expression of both FGF-2 and EGFP was observed in the infarct (Fig. 2A–C). Administration of pIRES-FGF2-EGFP plasmid increased the number of neural progenitor cells (Fig. 2D, 2E) in the lateral wall of the SVZ after MCA occlusion (Fig. 2F).

Gene therapy for stroke holds promise because of its ability to induce expression of desired molecules by cells for a long period. Gene transfer for neurotrophic factors (8), anti-apoptotic protein (9), and heat shock protein (10) can ameliorate ischemic brain damage when administered before or even after induction of ischemia. Post ischemic treatment could be given to stroke patients provided that efficacy and safety were proven. However, the viral vectors such as herpes simplex virus and adenovirus used in experimental stud-

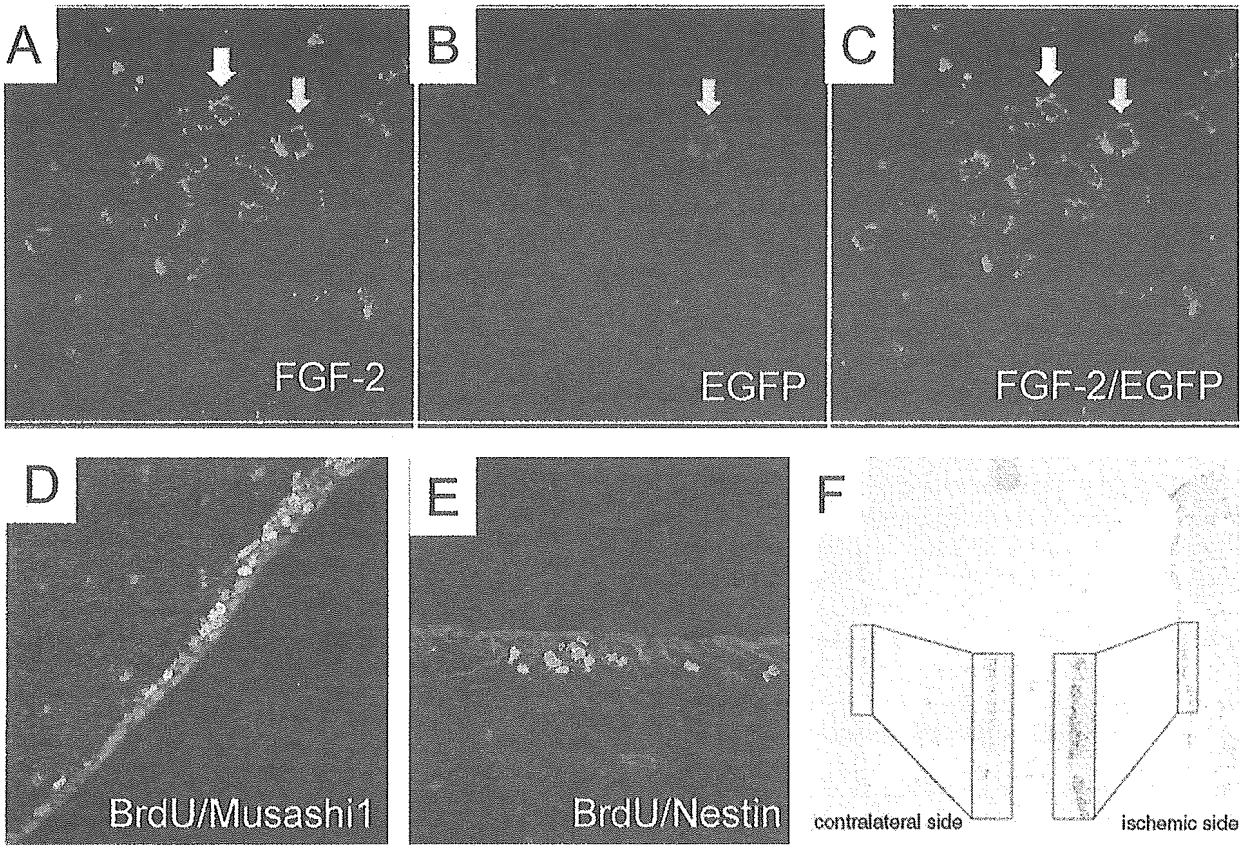


**Figure 2. Systemic administration of the pIRES-FGF2-EGFP plasmid resulted in expression of FGF-2 and EGFP in experimental cerebral infarction. After injection with pIRES-FGF2-EGFP, most EGFP-positive cells also expressed FGF-2 (A to C; yellow arrow). However, endogenous FGF-2 expression also was seen as FGF-2-positive and EGFP-negative cells (white arrow in A and C). (D, E) Neural stem/progenitor cells in the SVZ. Cells doubly positive for BrdU plus either marker of neural stem/progenitor cells, Musashi-1 (E) or nestin (F), were localized in the SVZ. (F) Effect of systemic administration of pIRES-FGF2-EGFP plasmid on BrdU incorporation in the SVZ *in vivo* is shown. The plasmid was injected after MCA occlusion. Note the marked increase in BrdU-positive cells in the SVZ on the ischemic side.**

ies, carry important potential problems such as toxic inflammatory responses, immunogenicity of virally infected cells, neoplastic transformation, relatively low DNA size limits, and difficulties in preparation. Furthermore, previous studies often have involved intracerebral, intrathecal, or intraventricular injection of the exogenous gene; such invasive gene delivery techniques are not practical for routine medical treatment in stroke patients. To date, neither viral nor nonviral methods have been effective in transfecting intact brain after intravenous delivery. The main advantages of nonviral methods including liposome-DNA complexes are safety, ease of preparation, and ability to deliver DNAs of unlimited size. Zhu et al (1993) (11), Liu et al (1997) (7), and Templeton et al (1997) (12) all reported that injection of plasmid DNA in cationic liposomes into the tail vein of mice could induce efficient gene transfer in several organs including lung, spleen, heart, kidney, and liver. Vascular endothelial cells, monocytes, and macrophages are the cell types most commonly transfected by intravenous injection of cationic liposome-DNA complexes. However, uptake by the endothelial cells was nearly absent in the brain. Although few macrophages are found in the intact brain, the circulating monocytes and other mononuclear blood cells accumulate in the brain and differentiate into microglia and macrophages once infarction develops (5). As novel cellular vehicles for gene therapy, the macrophages previously have been genetically modified *ex vivo* and reintroduced into the body with the hope that some of them will migrate selectively to the site of disease (13). When we used FGF-2 plasmid for systemic gene therapy, treatment increased numbers of neural progenitors in the SVZ on the ischemic side. It was previously shown that intracerebroventricular administration of FGF-2 protein or cDNA increased the numbers of the progenitor cells in the SVZ (4, 14). However, other neurotrophic factors such as epidermal growth factor may be more effective in enhancing neurogenesis after stroke.

The procedure we introduced will be attractive in stroke patients because it is essentially noninvasive. However, several technical problems such as nonspecific expression and low efficiency for the gene transfer need to be addressed in the future. Transcriptional targeting of the transgene using the macrophage-specific promoters or promoters of the genes up-regulated only within the cerebral infarct, may prove essential for avoiding unwanted side effects. It is well known that liposome-DNA complexes usually show low transfection efficiency *in vitro*. Modification of the cationic liposomes and the DNA to liposome ratio also might improve transfer efficiency. High-expression promoters could increase synthesis of the protein product, which might be otherwise insufficient when nonviral vectors are used for gene transfer.

In conclusion, we introduced intravenous delivery of the plasmid DNA to the macrophages infiltrating an experimental brain infarct in rats. Although further improvements in promoters for the expression vector, in liposomes complexed with the DNA, and in administration strategy will be required, systemic gene therapy using macrophages for *in vivo* targeting holds clinical promise in stroke patients, given its simplicity, safety related to the nonviral nature of the vector, and noninvasive mode of administration.

## References


1) Yagita Y, Kitagawa K, Ohtsuki T, et al. Neurogenesis by progenitor cells in the ischemic adult rat hippocampus. Stroke **32**: 1890–1896, 2001.
2) Arvidsson A, Collin T, Kirik D, Kokaia Z, Lindvall O. Neuronal replacement from endogenous precursors in the adult brain after stroke. Nat Med **8**: 963–970, 2002.
3) Jin K, Mao XO, Sun Y, Xie L, Greenberg DA. Stem cell factor stimulates neurogenesis in vitro and in vivo. J Clin Invest **110**: 311–319, 2002.
4) Nakatomi H, Kuriu T, Okabe S, et al. Regeneration of hippocampal pyramidal neurons after ischemic brain injury by recruitment of endogenous neural progenitors. Cell **110**: 429–441, 2002.
5) Mabuchi T, Kitagawa K, Ohtsuki T, et al. Contribution of microglia/macrophages to expansion of infarction and response of oligodendrocytes after focal cerebral ischemia in rats. Stroke **31**: 1735–1743, 2000.
6) Burke B, Sumner S, Maitland N, Lewis CE. Macrophages in gene therapy: Cellular delivery vehicles and in vivo targets. J Leukoc Biol **72**: 417–428, 2002.
7) Liu Y, Mounkes LC, Liggitt HD, et al. Factors influencing the efficiency of cationic liposome-mediated intravenous gene delivery. Nat Biotechnol **15**: 167–173, 1997.
8) Kitagawa H, Sasaki C, Sakai K, et al. Adenovirus-mediated gene transfer of glial cell line-derived neurotrophic factor prevents ischemic brain injury after transient middle cerebral artery occlusion in rats. J Cereb Blood Flow Metab **19**: 1336–1344, 1999.
9) Lawrence MS, Ho DY, Sun GH, Steinberg GK, Sapolsky RM. Overexpression of bcl-2 with herpes simplex virus vectors protects cns neurons against neurological insults in vitro and in vivo. J Neurosci **16**: 486–496, 1996.
10) Yenari MA, Fink SL, Sun GH, et al. Gene therapy with hsp72 is neuroprotective in rat models of stroke and epilepsy. Ann Neurol **44**: 584–591, 1998.
11) Zhu N, Liggitt D, Liu Y, Debs R. Systemic gene expression after intravenous DNA delivery into adult mice. Science **261**: 209–211, 1993.
12) Templeton NS, Lasic DD, Frederik PM, Strey HH, Roberts DD, Pavlakis GN. Improved DNA: Liposome complexes for increased systemic delivery and gene expression. Nat Biotechnol **15**: 647–652, 1997.
13) Griffiths L, Binley K, Iqball S, et al. The macrophage—a novel system to deliver gene therapy to pathological hypoxia. Gene Ther **7**: 255–262, 2000.
14) Kuhn HG, Winkler J, Kempermann G, Thal LJ, Gage FH. Epidermal growth factor and fibroblast growth factor-2 have different effects on neural progenitors in the adult rat brain. J Neurosci **17**: 5820–5829, 1997.

ORIGINAL RESEARCH

# Combinations of the Presence or Absence of Cerebral Microbleeds and Advanced White Matter Hyperintensity as Predictors of Subsequent Stroke Types

H. Naka
E. Nomura
T. Takahashi
S. Wakabayashi
Y. Mimori
H. Kajikawa
T. Kohriyama
M. Matsumoto

**BACKGROUND AND PURPOSE:** Previous studies have shown microbleeds to be a risk factor for intracerebral hemorrhage and white matter hyperintensity (WMH) to be a risk factor for ischemic stroke. This study was performed to determine whether combinations of the presence or absence of microbleeds and advanced WMH are risk factors for subsequent recurrent stroke types.

**METHODS:** In 266 patients with stroke, microbleeds on T2*-weighted MR images were counted, and WMH on T2-weighted images was graded. Patients were divided into 4 groups by the combinations of the presence or absence of microbleeds and advanced WMH and were followed up for stroke recurrence.

**RESULTS:** During a mean follow-up period of 564.8 ± 220.5 days, 26 patients developed recurrent strokes, including 10 intracerebral hemorrhages and 16 ischemic strokes. Patients with microbleeds without advanced WMH ($n$ = 42) developed only intracerebral hemorrhages ($n$ = 8), and the recurrence rate of intracerebral hemorrhage in those patients estimated by the Kaplan-Meier method was the highest in the 4 groups (14.3% in 1 year and 21.2% in 2 years). In contrast, patients with advanced WMH without microbleeds ($n$ = 39) developed only ischemic strokes ($n$ = 6), and the estimated recurrent rate of ischemic stroke in those patients was the highest in the 4 groups (10.5% in 1 year and 17.4% in 2 years). Cox proportional hazards regression analysis revealed that microbleeds were associated with intracerebral hemorrhage (hazard ratio [HR], 85.626; 95% confidence interval [CI], 6.344–1155.649) and that advanced WMH was negatively associated with intracerebral hemorrhage (HR, 0.016; 95% CI, 0.001–0.258). Advanced WMH was associated with ischemic stroke (HR, 10.659; 95% CI, 2.601–43.678).

**CONCLUSION:** It appears that patients at high risk of subsequent intracerebral hemorrhage or ischemic stroke can be identified by combinations of the presence or absence of microbleeds and advanced WMH.

Gradient-echo T2*-weighted MR imaging is an extremely sensitive technique for detecting silent microbleeds, which are shown as signal-intensity loss, representing hemosiderin deposit.[1,2] An association between the presence of microbleeds and the severity of white matter hyperintensity (WMH) has been revealed in many previous studies.[3-8] Although both cerebral microbleeds and WMH are associated with common risk factors, the main one being hypertension, and are associated with small-artery diseases, the presence of microbleeds has been reported to be a risk factor for intracerebral hemorrhage,[6-16] and WMH has been reported to be a risk factor for ischemic stroke.[17-20] However, to the best of our knowledge, there have been no prospective studies focusing on combinations of microbleeds and advanced WMH as predictors for subsequent stroke types. Therefore, we performed the present study to determine whether cerebral microbleeds and advanced WMH are risk factors for certain types of subsequent stroke, by focusing on the combinations of the presence or absence of these 2 types of small-artery disease.

Received July 16, 2005; accepted after revision August 31.

From the Departments of Neurology (H.N., T.T., Y.M.) and Neurosurgery (S.W., H.K.), Suiseikai Kajikawa Hospital; and the Department of Clinical Neuroscience and Therapeutics (E.N., T.K., M.M.), Hiroshima University, Graduate School of Biomedical Sciences.

This study was partially supported by research grants from the Ministry of Health, Labor and Welfare of Japan and from the Smoking Research Foundation of Japan.

Address correspondence to Hiromitsu Naka, MD, Department of Neurology, Suiseikai Kajikawa Hospital, 8-20 Showamachi, Naka-ku, Hiroshima 730-0046, Japan.

## Methods

Subjects for the present study were enrolled from outpatients of our hospital who had acute stroke treated at our hospital, had been continuously followed up after discharge, and underwent MR imaging studies during the period from July 2002 to June 2004. Diagnosis of acute stroke was made on the basis of neurologic signs and symptoms and on the basis of results of neuroradiologic examinations. Stroke was classified into ischemic stroke and intracerebral hemorrhage, and ischemic stroke was further classified according to the criteria of the National Institute of Neurologic Disorders and Stroke as atherothrombotic infarction, cardioembolic infarction, and lacunar infarction.[21] Among patients with ischemic stroke, those with lacunar infarction and atherothrombotic infarction were included and those with cardioembolic infarction or undetermined classification were excluded from this study. In addition, among patients with intracerebral hemorrhage, cases were restricted to those in which the hematoma was present in the pons, cerebellum, thalamus, or putamen. Cases in which the hematoma was present in the subcortical lesion and those in whom hematoma was not caused by spontaneous intracerebral hemorrhage (eg, caused by vascular malformation, trauma, cavernous angioma, or brain tumor) were excluded.

Hypertension was defined as systolic blood pressure of ≥140 mm Hg and diastolic blood pressure of ≥90 mm Hg and included patients currently undergoing medical treatment for hypertension. Diabetes mellitus was defined as a glycosylated hemoglobin A1c concentration of >5.8% and included patients currently using hypoglycemic agents. Hypercholesterolemia was defined as a total cholesterol level